Mineralium Deposita (2006) 40: 802–827
DOI 10.1007/s00126-005-0013-y

ARTICLE

Kevin Faure · Robert L. Brathwaite

Mineralogical and stable isotope studies of gold–arsenic mineralisation in the Sams Creek peralkaline porphyritic granite, South Island, New Zealand

Received: 9 July 2004 / Accepted: 27 July 2005 / Published online: 19 January 2006

Abstract At Sams Creek, a gold-bearing, peralkaline granite porphyry dyke, which has a 7 km strike length and is up to 60 m in thickness, intrudes camptonite lamprophyre dykes and lower greenschist facies metapelites and quartzites of the Late Ordovician Wangapeka formation. The lamprophyre dykes occur as thin (< 3 m) slivers along the contacts of the granite dyke. $\delta^{18}O_{magma}$ values (+5 to +8‰, VSMOW) of the A-type granite suggest derivation from a primitive source, with an insignificant mature crustal contribution. Hydrothermal gold–sulphide mineralisation is confined to the granite and adjacent lamprophyre; metapelite country rocks have only weak hydrothermal alteration. Three stages of hydrothermal alteration have been identified in the granite: Stage I alteration (high fO_2) consisting of magnetite–siderite ± biotite; Stage II consisting of thin quartz–pyrite veinlets; and Stage III (low fO_2) consisting of sulphides, quartz and siderite veins, and pervasive silicification. The lamprophyre is altered to an ankerite–chlorite–sericite assemblage. Stage III sulphide veins are composed of arsenopyrite + pyrite ± galena ± sphalerite ± gold ± chalcopyrite ± pyrrhotite ± rutile ± graphite. Three phases of deformation have affected the area, and the mineralised veins and the granite and lamprophyre dykes have been deformed by two phases of folding, the youngest of which is Early Cretaceous. Locally preserved early-formed fluid inclusions are either carbonic, showing two- or three-phases at room temperature (liquid CO_2-CH_4 + liquid H_2O ± CO_2 vapour) or two-phase liquid-rich aqueous inclusions, some of which contain clathrates. Salinities of the aqueous inclusions are in the range of 1.4 to 7.6 wt% NaCl equiv. Final homogenisation temperatures (Th) of the carbonic inclusions indicate minimum trapping temperatures of 320 to 355°C, which are not too different from vein formation temperatures of 340–380°C estimated from quartz–albite stable isotope thermometry. $\delta^{18}O$ values of Stage II and III vein quartz range from +12 and +17‰ and have a bimodal distribution (+14.5 and +16‰) with Stage II vein quartz accounting for the lower values. Siderite in Stage III veins have $\delta^{18}O$ (+12 to +16‰) and $\delta^{13}C$ values (−5‰, relative to VPDB), unlike those from Wangapeka Formation metasediments ($\delta^{13}C_{bulk\ carbon}$ values of −24 to −19‰) and underlying Arthur Marble marine carbonates ($\delta^{18}O$ = +25‰ and $\delta^{13}C$ = 0‰). Calculated $\delta^{18}O_{water}$ (+8 to +11‰, at 340°C) and $\delta^{13}C_{CO_2}$(−5‰) values from vein quartz and siderite are consistent with a magmatic hydrothermal source, but a metamorphic hydrothermal origin cannot be excluded. $\delta^{34}S$ values of sulphides range from +5 to +10‰ (relative to CDT) and also have a bimodal distribution (modes at +6 and +9‰, correlated with Stage II and Stage III mineralisation, respectively). The $\delta^{34}S$ values of pyrite from the Arthur Marble marine carbonates (range from +3 to +13‰) and Wangapeka Formation (range from −4 to +9.5‰) indicate that they are potential sources of sulphur for sulphides in the Sams Creek veins. Another possible source of the sulphur is the lithospheric mantle which has positive values up to +14‰. Ages of the granite, lamprophyre, alteration/mineralisation, and deformation in the region are not well constrained, which makes it difficult to identify sources of mineralisation with respect to timing. Our mineralogical and stable isotope data does not exclude a metamorphic source, but we consider that the source of the mineralisation can best be explained by a magmatic hydrothermal source. Assuming that the hydrothermal fluids were sourced from crystallisation of the Sams Creek granite or an underlying magma chamber, then the Sams Creek gold deposit appears to be a hybrid between those described as reduced granite Au–Bi deposits and alkaline intrusive-hosted Au–Mo–Cu deposits.

Keywords Granite · Peralkaline · Porphyry · Gold · Arsenic · Isotope

Communicated by Editorial handling: J. Richards

K. Faure (✉) · R. L. Brathwaite
GNS Science, P.O. Box 30-368, Lower Hutt, New Zealand
E-mail: k.faure@gns.cri.nz

Introduction

Gold mineralisation at Sams Creek, 25 km south of Takaka in the northwest Nelson region of the northern part of the South Island of New Zealand (Fig. 1), was discovered in 1974 by CRA Exploration (CRAE). From 1980 to 1987 CRAE (e.g. Clemenston 1987) undertook a programme of geological mapping, geochemical sampling, geophysical surveys and diamond drilling (42 drill holes). Thirty of these drill holes tested a 1 km strike length of the dyke at Main Zone prospect, and indicated that a bulk mining target of 2 to 3 g/t Au was possible. Oceana Gold Ltd have completed 12 diamond drill holes since 2002 in the Main Zone (Reynolds 2004) defining an inferred resource of 13.5 Mt @ 1.78 g/t Au containing 776,000 ounces of gold (0.7 g/t cut-off; Oceana Gold Ltd 2004).

Gold is associated with arsenopyrite–pyrite–quartz–siderite mineralisation in a peralkaline granite porphyry dyke which intrudes Lower Palaeozoic metasedimentary rocks. The granite dyke has a thickness of 30 to 60 m, and extends discontinuously for 7 km (Fig. 2). Thin dykes (< 3 m) of altered lamprophyre occur locally along the margins of the granite dyke and also contain arsenopyrite–pyrite–carbonate veins. Arsenopyrite–pyrite–carbonate veins are absent from the metasedimentary country rocks.

In the first published record of the dyke, Shelley (1984) noted that it was a metamorphosed riebeckite microgranite. Windle and Craw (1991) considered that the granite dyke had been buckled and dismembered by folding, and concluded that the mineralising fluids were of metamorphic origin (orogenic gold) and suggested that the mineralisation was confined to the granite porphyry dyke because of its distinctive Fe^{3+}-rich composition. Tulloch (1992) described the mineralogy and chemistry of the granite as peralkaline and noted that the granite was altered by late and/or postmagmatic fluids. Our preliminary studies indicated that the ore mineralogy, hydrothermal alteration, and stable isotope compositions of the vein minerals at the Sams Creek

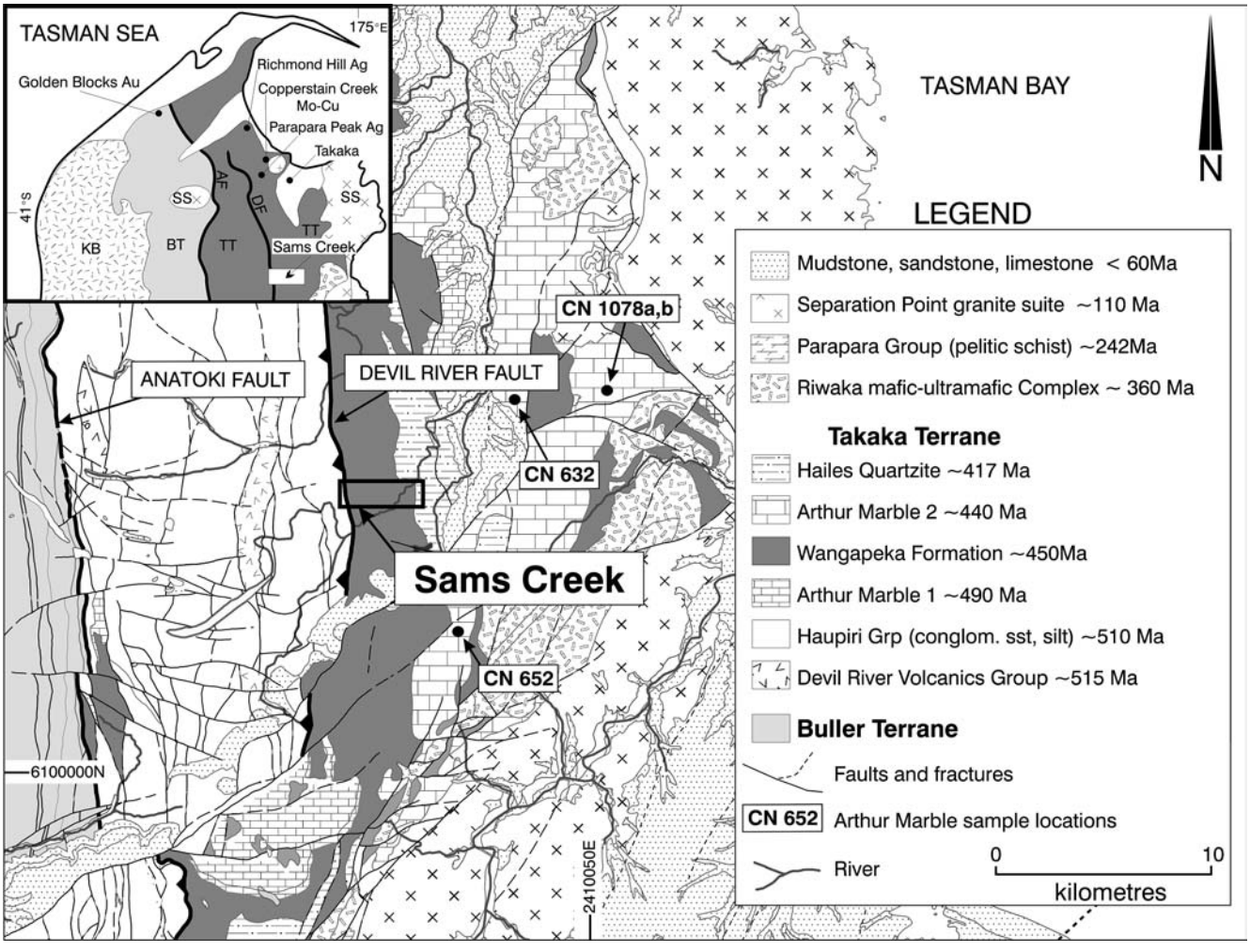

Fig. 1 Regional geology map of the Sams Creek area (modified after Rattenbury et al. 1998). Inset: Regional location map of Sams Creek area in the north of the South Island, New Zealand. *BT* Buller Terrane; (*TT*) Takaka Terrane; (*KB*) Karamea Granite Batholith; (*SS*) Separation Point Suite Granitoids; (*RC*) Riwaka Complex; (*AF*) Anatoki Fault; (*DF*) Devil River Fault

gold deposit are similar to other granite-related gold deposits, but that it appears to be a variant of the alkaline intrusion-related gold deposit type—an As–Au deposit associated with a peralkaline granite and lamprophyre (Faure et al. 2003; Brathwaite and Faure 2004).

Here, we present detailed mineralogical, fluid inclusion and isotope data to establish which is the most likely source of the gold–sulphide mineralisation at Sams Creek–magmatic hydrothermal or metamorphic hydrothermal.

Regional setting

The Sams Creek area lies in the Takaka Terrane (Fig. 1), a belt of Lower Paleozoic metasedimentary rocks in northwest Nelson (Grindley 1978, 1980; Cooper 1989; Rattenbury et al. 1998). The Takaka Terrane is structurally complex and is preserved in a series of north-trending fault-bound slices (Cooper and Tulloch 1992; Münker and Cooper 1999). The Devil River Fault divides the Takaka Terrane into western and eastern parts, with the Cambrian arc–related Haupiri and Devil River Volcanics Groups to the west, and the Ordovician to Early Devonian passive margin sequence of the Wangapeka Formation, Arthur Marble, Hailes Quartzite and Baton Formation to the east (Fig. 1).

The Takaka Terrane has been intruded by the Late Devonian Riwaka mafic-ultramafic complex and I-type granites of the Early Cretaceous (~110 Ma) Separation Point Suite (Tulloch 1983; Muir et al. 1995; Muir et al. 1996; Tulloch et al. 2003). Recent unpublished Ar–Ar data indicate that the age of the Sams Creek granite dyke is about 319 Ma (see below). Three phases of deformation have been identified in the region: a first phase of recumbent folding (F_1), a second of inclined folds (F_2) about sub-horizontal north–south trending axes, and a third (F_3) of localised northeast to southeast trending folds (Grindley 1980; Jongens 1997). According to Bradshaw (2000), the Early Devonian Baton Formation is affected by the F_1 and F_2 folding, and the F_1 cleavage is cut by mafic dykes that may be related to the Late Devonian Riwaka Complex. However, the correlation of the mafic dykes with the Riwaka complex is uncertain and Grindley (1980) noted a strong foliation along the margins of the Riwaka Complex, which may be associated with syn-emplacement deformation. Bradshaw (2000) was uncertain as to whether the F_2 folds pre-dated the Late Devonian intrusives. Jongens (1997, 2004) relates the F_1 and F_2 deformations to tectonic shortening associated with the amalgamation of Takaka and Buller terranes. Radiometric dating indicates that a northeast-trending regional schistosity in the area northwest of Takaka, which is correlated with F_3 deformation, was associated with the emplacement of the voluminous Separation Point batholith in the Early Cretaceous (Challis et al. 1995). The region has also been affected by late Tertiary and Quaternary folding and faulting, as indicated by deformation of mid-Tertiary sedimentary rocks which unconformably overlie the older rocks.

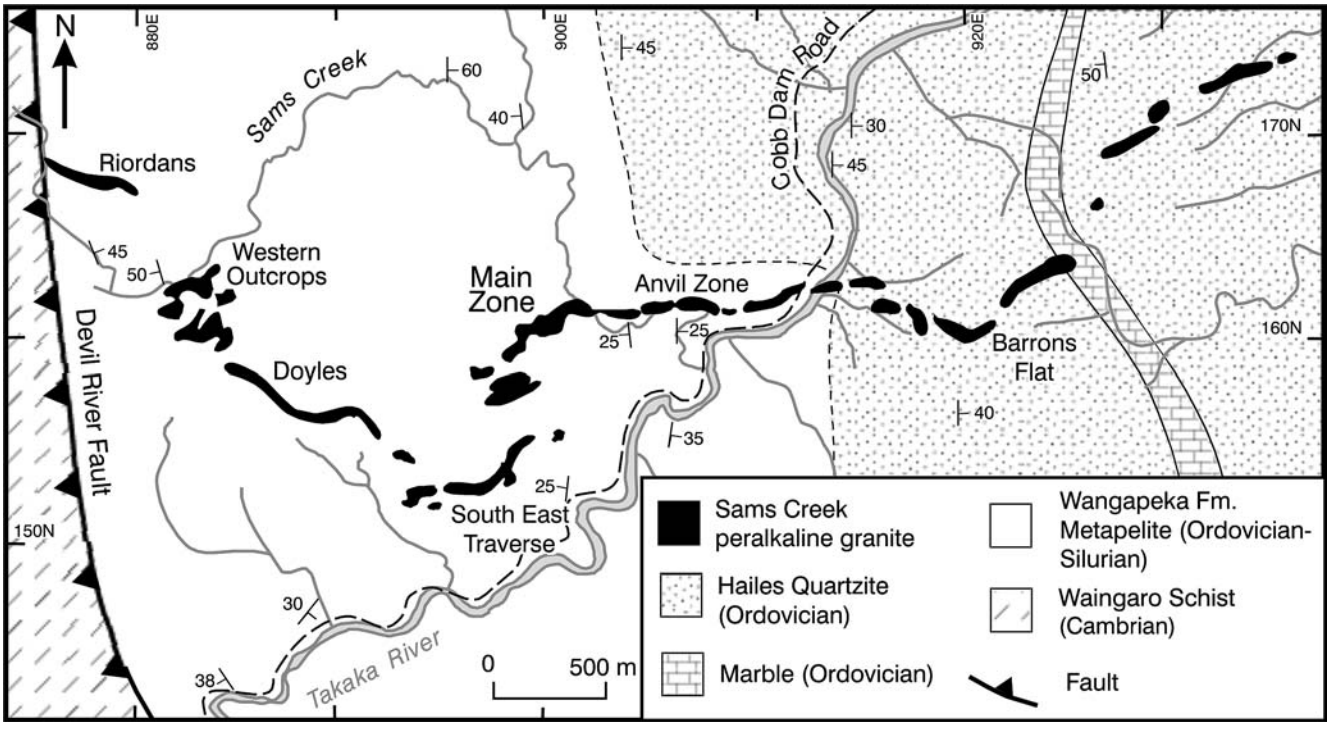

Fig. 2 Geological map of the Sams Creek area, Upper Takaka. Adapted from CRA Exploration mapping (Clementson 1987) by Tulloch (1992), with additional data from Hickey (1986)

The Paleozoic mineral deposits of northwest Nelson include: orogenic gold–quartz lodes (Golden Blocks) hosted in Ordovician metagreywackes and slates of the Buller Terrane and Ni–Cu sulphide mineralisation in gabbro and pyroxenite of the Riwaka Complex (Brathwaite and Pirajno 1993; Fig. 1). Granite-related mineralisation other than Sams Creek comprises: (a) silver-bearing quartz–sulphide veins associated with granite porphyries at Richmond Hill and Parapara Peak, (b) a weakly schistose granodiorite porphyry of Early Cretaceous (133.5 Ma) age associated with molybdenite and a magnetite–pyrite–chalcopyrite skarn at Copperstain Creek (Brathwaite et al. 2004), and (c) porphyry-style molybdenite mineralisation associated with granodiorite stocks of high Na and Sr/Y chemistry belonging to the 126–105 Ma Separation Point Suite granitoids (Tulloch and Rabone 1993; Tulloch and Kimbrough 2003).

Deposit geology

Sams Creek is a deeply incised tributary of the Takaka River (Fig. 2). The Sams Creek granite porphyry, which hosts the gold–sulphide mineralisation, intrudes the Ordovician-Silurian Wangapeka Formation (Mount Arthur Group), which consists of metapelites and quartzites with several marble bands (Grindley 1980; Cooper 1989; Rattenbury et al. 1998). These metasedimentary rocks overlie the Early Ordovician Arthur Marble 1 (Cooper 1989). Although, the general sequence is similar throughout the Takaka terrane, there are variations between areas and within fault slices. It is possible that the Sams Creek granite may have intruded older sequences below the Mount Arthur Group, such as the calcareous siltstones/sandstones of the Mount Patriarch Group, which is not exposed in the Sams Creek area. The Sams Creek granite body, which extends discontinuously for about 7 km, has been arbitrarily divided into the Riordans, Western Outcrops, Doyles, South East Traverse, Main Zone, Anvil Zone and Barrons Flat zones (Fig. 2). Its broadly linear orientation and discordance to bedding in the metasedimentary rocks indicate that it is a dyke.

The metasedimentary rocks have been folded and regionally metamorphosed to a lower greenschist facies assemblage of quartz–albite–muscovite–chlorite. Shelley (1984) described a recumbent fold (F_1) at Sams Creek which has been refolded by northerly trending F_2 folds. Hickey (1986) mapped the F_2 folds as being inclined with sub-horizontal axes and also identified F_3 folding about steeply plunging axes. The granite dyke cuts the F_1 folds at high angles, and therefore postdates the F_1 deformation. A prominent crenulation cleavage is axial planar to the F_2 folds (Shelley 1984; Hickey 1986; Windle and Craw 1991), and this cleavage also extends into hydrothermally altered lamprophyre, which in places occurs along the margins of the granite dyke. In the Anvil section (Fig. 2), Windle and Craw (1991) mapped deflection of the cleavage around the margins of granite bodies that have been dismembered by deformation. This, together with the sinuous outcrop pattern of the granite dyke and the presence of extensive shearing in the dyke and along many of its contacts, indicate that it has been deformed and folded by the F_2 and F_3 events.

Relatively, unaltered granite porphyry is a speckled grey to pinkish-grey rock, with phenocrysts of perthite (0.5–5 mm in length), dark arfvedsonite (sodic amphibole), green aegerine (sodic pyroxene), and quartz (up to 4 mm) in a hypidiomorphic granular (c. 0.2 mm) aggregate of perthite, quartz, plagioclase, arfvedsonite, and aegerine. Myrmekitic intergrowths of quartz and plagioclase are also present. Ilmenite, rutile and fluorite are accessory minerals. The arfvedsonite is partly replaced by rims of riebeckite. The sodic mineralogy, low Al_2O_3 and Sr, coupled with high Zr, Nb, Ga and Y, are characteristic of peralkaline ($Na_2O + K_2O > Al_2O_3$) A-type granites (Tulloch 1992). The presence of ilmenite, absence of primary magnetite, and a low-magnetic susceptibility (30 SI units$\times 10^{-5}$) in the least-altered granite classifies it as a reduced, (low fO_2) granite (Ishihara 1981).

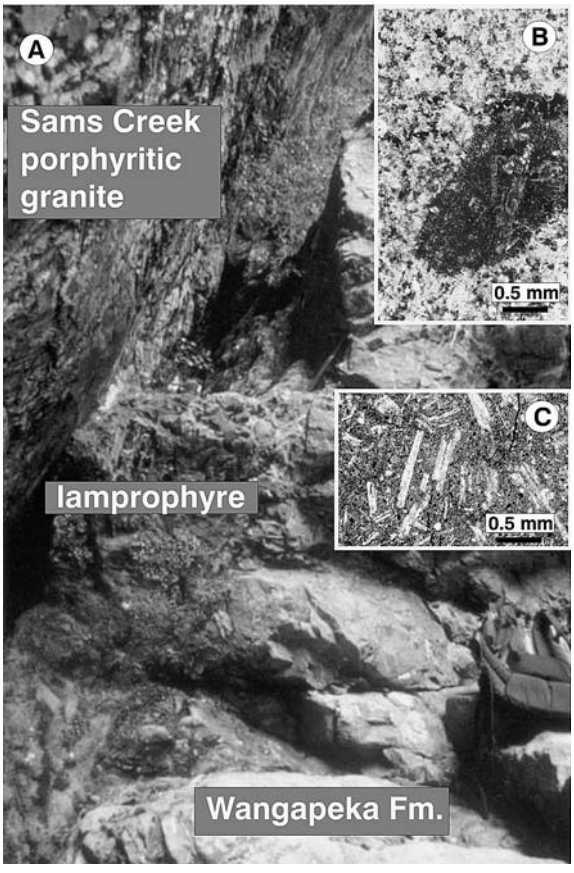

Fig. 3 **a** Outcrop photo of Sams Creek granite-lamprophyre-Wangapeka Formation contact. **b** Photomicrograph (transmitted plane polarised light) of altered lamprophyre xenolith in altered microgranite. **c** Photomicrograph (transmitted plane light) of altered lamprophyre with relict plagioclase laths in a fine-grained ankerite-sericite rich groundmass

Thin (< 3.0 m) dykes of lamprophyre occur along the contacts of the granite porphyry dyke (Fig. 3a) and in the adjacent metapelite. In the Main Zone, the lamprophyre dykes appear to be thicker along the northern contact of the granite porphyry dyke. Contacts of the lamprophyre and metapelite are commonly sheared, but in some cases a sharp contact has been preserved and a crenulation cleavage extends from the metapelite into the altered lamprophyre, where it is defined by alignment of sericite crystals. The presence of lamprophyre dykes at, and concordant with, the margins of the granite dike (Fig. 3a) and the occurrence of inclusions of lamprophyre in the granite (Fig. 3b) adjacent to its contacts with lamprophyre suggests that the lamprophyre dykes were intruded before the granite dyke and along the same fracture as the granite. In most cases the lamprophyre is altered to an ankerite–chlorite–sericite assemblage, but least altered samples of the lamprophyre contain relict phenocrysts of plagioclase (Fig. 3c), titaniferous augite, brown amphibole, biotite, magnetite, ilmenite, and apatite. The mineralogy and chemical analyses of the lamprophyre indicate that it is a camptonite (Windle 1989; Windle and Craw 1991).

Despite high Zr contents of 1,180–1,380 ppm, the granite contains insignificant amounts of zircon and several attempts to separate this mineral for U–Pb dating have been unsuccessful. K–Ar dates of amphibole from the granite are 226 ± 1.1 Ma (Tulloch 1992), and 246 ± 3 Ma (Tulloch (personal communication)), but these are probably minimum ages due to resetting during the thermal and deformation events that have affected the area. Recent Ar–Ar data for a sample of arfedsonite–reibeckite from the granite show a disturbed staircase spectrum, with an interpreted age of 319 ± 8 Ma (Tulloch and Dunlap submitted). This age correlates with the ages (320–292 Ma, Tulloch et al. 2003) of other localised A-type granites such as the Foulwind granite, ~150 km southwest of Sams Creek and Freds Camp granite on Stewart Island. However, these other A-type granites have a peraluminous rather than peralkaline composition. There are extensive Early Cretaceous granitoids in the Northwest Nelson region (see "Regional Setting"), but they are all I-Type granites. In summary, the Sams Creek peralkaline granite has not been positively linked with any of the known magmatic events in this part of New Zealand.

Table 1 Average concentration (ppm per one-metre core-length) for elements from drillcore (SC43, 44, 45 and, 48; data provided by Oceana Gold Ltd). These are averages for samples from Sams Creek granite and lamprophyre. Samples from host metapelites are below limits of detection (Fig. 6)

	Au	Ag	As	Zn	Pb	Cu	Mo	Bi
Average	1.8	1.1	6972.0	323.8	147.8	16.1	5.6	0.4
N	260	249	249	249	249	249	249	249
Max	9.2	34.5	43,500	4,350	2,050	320	26	6.5
Min	0	0	0	40	1.5	1	1	0

Analytical methods and samples

Samples

Samples in this study are largely from drill core provided by Oceana Gold Ltd. Only the Main Zone at Sams Creek has been systematically drilled to date, due mainly to the steep topography and difficult access (Fig. 1). Therefore, most of the samples in this study are from drill core from the Main Zone, but some drill core samples from the other sections drilled by CRA, and Sams Creek granite outcrop samples were also analysed. Sample descriptions and localities are listed in Appendix I.

Sample selection, particularly for stable isotope analyses, was an important part of this study, because of possible isotope re-equilibration effects as a consequence of recrystallisation. In determining which samples were to be analysed, care was taken to sample minerals that did not appear to be recrystallised, i.e. they have no subgrains or fine grained overgrowths, no ribbon textures and only a low density of microcracks. Granite quartz and feldspar phenocrysts were sampled from thin section and more than one phenocryst per sample was analysed to ascertain isotope heterogeneity. Granite feldspar phenocrysts and groundmass were generally hydrothermally altered (discussed below). Outcrop samples (P43154, P68912, P68913, P68914, P68914a) of Sams Creek granite that show no apparent evidence of alteration of feldspar were collected from localities outside of the Main Zone. Arthur Marble samples that contained trace amounts of pyrite were provided by John Simes (GNS Science, Lower Hutt; sample locations plotted on Fig. 1). Pyrite cubes (0.1–2 mm) were obtained from the marble by dissolution of the carbonate by acetic acid.

Whole-rock geochemical analyses

Geochemical analyses of selected elements from intersections of the granite and lamprophyre dykes and metasediments in four drill holes (SC43, 44, 45 and 48) have been provided by Oceana Gold Ltd for this study. One-metre-long drill core samples were analysed for Au by fire assay and Ag, As, Cu, Pb, Zn, Mo and Bi by inductively coupled plasma mass spectroscopy (ICP-MS). Au was analysed at the Amdel laboratory, Macraes mine site, and the rest of the elements were analysed at the Amdel laboratory, Adelaide. A summary of the results are listed in Tables 1 and 2.

Mineral analyses

Gold and carbonate minerals were analysed using a Jeol Superprobe 733 electron probe microanalyser (EPMA) at Victoria University of Wellington, New Zealand. For

Table 2 Correlation (R^2) of elements in Sams Creek granite and lampropyhre

	Ag	As	Cu	Pb	Zn	Mo	Bi
Au	0.28	0.75	0.00	0.32	0.21	0.07	0.16
Ag		0.26	0.81	0.25	0.22	0.46	0.06
As			0.08	0.24	0.11	0.17	0.12
Cu				0.13	0.17	0.48	−0.03
Pb					0.17	0.48	−0.03
Zn						0.48	−0.03
Mo							−0.03

carbonate analyses operating conditions were 15 kV with a beam current of 12 nA using synthetic metal oxide standards. For gold analyses operating conditions were 25 kV with a beam current of 15 nA using pure metal (Au, Ag, Sb, Cu and Bi) standards. Analyses are listed in Table 3 carbonates) and Table 4 (gold). Gold was analysed for in a selection of arsenopyrite grains, but was below the detection limit of 0.01 wt%.

Stable isotope analyses

Carbonate samples were microdrilled from drill core samples, crushed to a fine powder, and reacted in 105% H_3PO_4 at 80°C in an automated GEO20-20/CAPS system. An appropriate Δ CO_2-H_3PO_4 correction was applied to oxygen isotope ratios (McCrea 1950; Rosenbaum and Sheppard 1986). Carbonate sample values were normalised to the international calcite standard (NBS 19), $\delta^{18}O$ values are reported relative to VSMOW, and $\delta^{13}C$ values relative to VPDB. All isotope values are reported in the familiar per mil (‰) notation relative to the appropriate standard. Replicates of carbonate standards were better than 0.1‰ for carbon and oxygen values. Whole-rock carbon isotope analyses of metapelites were measured using the method of Boutton (1991). Samples were normalised to the oxalic-acid standard (SRM-4990) assuming a value of −19.3‰ (PDB). Oxygen isotope values of silicate samples were obtained using the laser ablation-BrF_5 method of Sharp (1990). Values of samples were normalised to the quartz standard NBS 28 assuming a value of 9.6‰ (VSMOW), with replicates usually better than 0.1‰ and always better than 0.2‰ (except feldspar phenocrysts–see below). Sulphur isotope values of sulphide samples were obtained using the methods of Robinson and Kusakabe (1975) and Sasaki et al. (1979). Sample values were normalised to an internal GNS pyrite standard (R2268) with replicate values typically better than 0.2‰. The $\delta^{34}S$ values are reported relative to CDT. Pyrite and chalcopyrite ($+Cu_2O$) were combusted at 1,000°C online and SO_2 measured for its $^{34}S/^{32}S$ ratio. Arsenopyrite was reduced by Kiba reagent to form H_2S, which was precipitated as Ag_2S and then combusted with Cu_2O to form SO_2. Finally, sphalerite was reacted with 1:1 HCl to form H_2S, which was precipitated as Ag_2S and then combusted with Cu_2O to form SO_2.

Alteration, mineralisation, and deformation

The Wangapeka Formation has been regionally metamorphosed to a lower greenschist facies assemblage of quartz–albite–muscovite–chlorite, but only local carbonate–sericite–pyrite hydrothermal alteration has been observed adjacent to the granite contact. Hydrothermal gold–sulphide mineralisation is confined to the Sams Creek granite and adjacent lamprophyre. Three stages of alteration and associated mineralisation are recognised in the granite, but only one stage can be identified in the lamprophyre. The alteration and mineralisation in the granite dyke is best documented at Main Zone, which is where by far the most drilling has been done.

The first stage of alteration (Stage I) is represented by a magnetite–ankerite ± biotite assemblage (Fig. 4a), which appears to be confined to the Main and adjacent Anvil Zones except for one sample from Barrons Flat. The magnetite–ankerite alteration consists mainly of subhedral to euhedral magnetite and ankerite grains that

Table 3 EMPA analyses of carbonate minerals from the Sams Creek gold deposit

Drill hole	SC26	SC44	SC48	SC42	SC45	SC45	SC48
Depth (m)	121.8	234	221.3	229.2	112.2	65.2	228.25
Analysis#	6	1	3	2	2	1	1
Habit	cb alt gran	vein gran	vein gran	mag alt gran	cb alt lamp	cb alt lamp	vein lamp
Mineral	siderite	siderite	siderite	siderite	siderite	ankerite	ankerite
FeO (%)	54.3	53.8	56.2	52.2	43.3	17.0	20.9
MnO	3.8	2.8	1.7	2.5	0.9	0.5	0.7
MgO	1.3	1.0	1.6	4.6	14.3	11.0	7.9
CaO	0.8	3.1	0.8	1.6	0.5	28.0	26.3
Total	60.2	60.8	60.3	60.9	58.9	56.6	55.8
FeCO3	93.4	86.8	90.6	84.2	69.8	28.1	33.7
MnCO3	2.2	4.6	2.8	4.0	1.5	0.5	1.1
MgCO3	2.8	2.1	3.3	9.7	29.3	25.6	16.5
CaCO3	1.6	5.5	1.4	2.8	0.8	46.7	46.9
Total	100.0	99.0	98.1	100.8	101.9	100.8	98.3

Abbreviations: alt alteration; *cb* carbonate; *gran* granite; *lamp* lamprophyre; *mag* magnetite

Table 4 Representative EMPA analyses of gold/electrum from the Sams Creek gold deposit

Sample	Ag wt%	Au wt%	Bi wt%	Total wt%
SC26-121.8-I	17.6	80.1	0.7	98.4
SC26-121.8-2	19.3	78.1	0.7	98.1
SC26-121.8-3	17.2	81.9	0.7	99.9
SC26-121.8-5	19.3	78.1	0.7	98.1
SC44-184.6-1	29.4	68.1	0.5	98.0
SC44-184.6-2	29.1	69.7	0.7	99.6
SC44-184.6-4	30.0	69.1	0.4	99.5
SC45-69.7-1	16.1	83.1	0.8	99.9
SC45-69.7-2	15.8	83.0	1.1	99.9
SC48-221.3-1	19.8	77.5	0.7	98.0

are clustered in and around the remnants of arfvedsonite and aegerine phenocrysts. In some samples the magnetite and ankerite are accompanied by fine-grained brown biotite. A few samples also contain traces of fine-grained chalcopyrite associated with magnetite. The occurrence of the early stage alteration minerals, magnetite and biotite, is similar to the magnetite + biotite alteration found in many calc-alkaline and alkaline porphyry Cu–Mo–Au deposits, where it represents an early high temperature stage (e.g. Sillitoe 2000; Jensen and Barton 2000 and references therein).

The second stage of alteration/mineralisation (Stage II) consists of thin quartz, pyrite, quartz-pyrite, or quartz–albite veinlets, which contain no gold (Fig. 4). Where these veinlets are contained in schistose microgranite, they also have schistose textures. The second stage quartz or quartz–pyrite veinlets are generally discontinuous due to disruption by shear/cleavage surfaces, but in least-deformed samples they are planar to semiplanar. They are cut by the third stage of gold-bearing sulphide and quartz–siderite veins (Stage III).

Stage III alteration/mineralisation consists of irregular to planar gold-bearing arsenopyrite–pyrite ± quartz–siderite ± sericite veins, which locally form vein stockworks (Fig. 4). Stage III mineralisation is most extensive at Main Zone and Anvil, but minor arsenopyrite–pyrite ± galena ± sphalerite–quartz–siderite–sericite veins also occur in the granite dyke at Riordans, Western Outcrops, Doyles, and Barrons Flat. Drill hole intersections from the Main Zone show that the sulphide–Au–quartz–siderite mineralisation can extend over the full width of the dyke (Fig. 6), although some other intersections are only sporadically mineralised. The veins are commonly sulphide rich and consist of semi-massive to massive aggregates of arsenopyrite with generally lesser pyrite, minor galena and sphalerite, and local gold. They vary in thickness from < 1 to 15 mm. Chalcopyrite is locally present in minor amounts (Fig. 5b). Minor rutile occurs locally in association with vein arsenopyrite, pyrite and quartz. Traces of pyrrhotite occur as small inclusions in pyrite and arsenopyrite (Fig. 5c), and crystalline graphite occurs locally in a number of samples (Fig. 5d). No bismuth minerals or molybdenite were found in any of the polished thin sections, which is

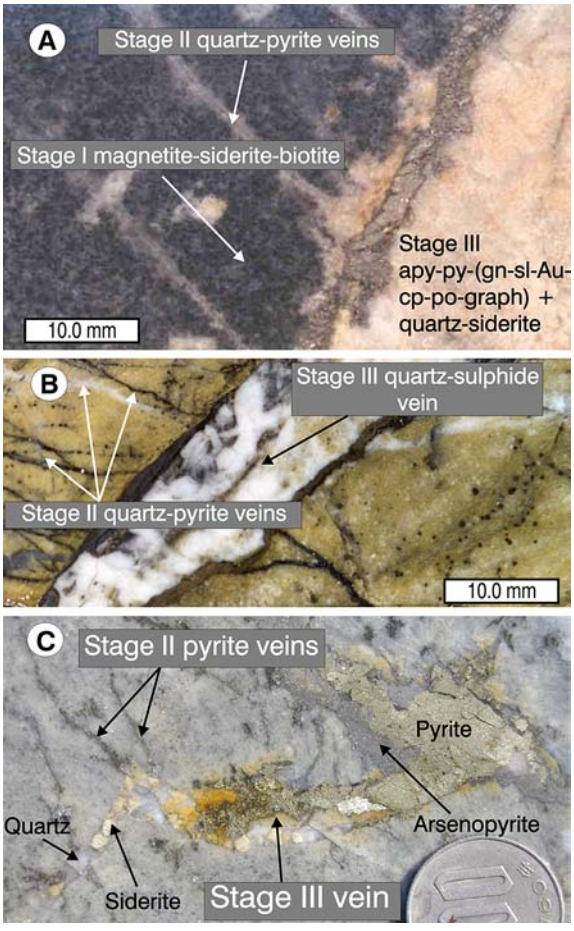

Fig. 4 Examples of the three different stages of alteration/mineralisation (relatively undeformed) observed in Sams Creek granite. Stage I magnetite-siderite ± biotite altered granite (mottled black), Stage II thin quartz-pyrite veins, Stage III arsenopyrite-pyrite-(galena-sphalerite-gold-chalcopyrite-pyrrhotite-graphite), quartz and siderite veins. **a** All three stages represented. **b** and **c** Stages II and III. *Abbreviations*: *apy* arsenopyrite; *py* pyrite; *gn* galena; *sl* sphalerite; *Au* gold; *cp* chalcopyrite; *po* pyrrhotite; *graph graphite*

consistent with low values of these elements in the drill hole assay data (Table 1). Vein assemblages containing sericite are uncommon in samples from the Main Zone, whereas at Riordans and Western Outcrops, a quartz–sericite–siderite assemblage is extensive. A K–Ar date of 101 ± 2 Ma on a sericite-altered granite sample from Western Outcrops may represent either the age of the hydrothermal alteration, or more likely a closure temperature for muscovite/sericite following uplift after the Early Cretaceous thermal event that has affected the region (Tulloch 1992; Tulloch and Dunlap submitted).

Adjacent to the Stage III sulphide–quartz–siderite veins, the granite is pervasively silicified to a quartz–perthite–albite–rutile ± pyrite–siderite ± sericite assemblage. Remnant arfvedsonite and aegerine are replaced by siderite, and the Stage I magnetite is replaced by pyrite and rutile. The lamprophyre dykes are altered to an ankerite–chlorite–sericite–titanite/leucoxene assemblage, which, allowing for their much more mafic

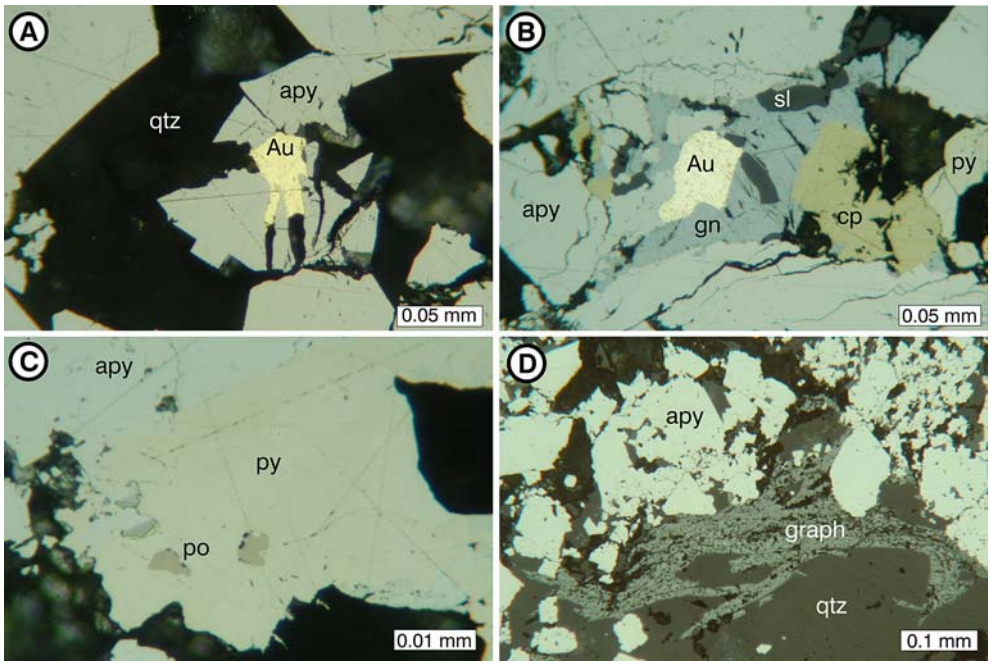

Fig. 5 Ore minerals. **a** Gold with arsenopyrite and quartz. **b** Gold associated with galena, chalcopyrite and sphalerite with arsenopyrite and pyrite. **c** Pyrrhotite inclusions in pyrite with arsenopyrite. **d** Crystalline graphite with arsenopyrite and quartz. Photomicrographs in reflected light. Abbreviations: *apy* arsenopyrite; *Au* gold; *cp*chalcopyrite; *gn* galena; *graph* graphite; *qtz* quartz; *py* pyrite; *po* pyrrhotite; *sl* sphalerite

composition than the microgranite, is similar to the third stage alteration seen in the microgranite. Country rock metapelites are only locally altered to a carbonate–sericite–pyrite assemblage along dike contacts, and show no evidence of contact metamorphism.

Gold is largely confined to the granite dyke. The altered lamprophyre locally contains carbonate–arsenopyrite–pyrite–sphalerite–galena veins with gold values of up to 0.82 g/t in drill core analyses. Gold (2–100 μm in size) is associated with the Stage III arsenopyrite–pyrite veins, where it occurs mainly in arsenopyrite (Fig. 5a). Within arsenopyrite crystals it is commonly in contact with inclusions of galena (Fig. 5b). Less frequently, gold occurs as small grains (5–10 μm) in vein quartz adjacent to arsenopyrite. The colour of the gold shows some variation from medium to pale yellow, suggesting that it contains significant silver (Table 4).

The Sams Creek granite and sulphide, carbonate and quartz veins have been variably deformed and recrystallised. Quartz crystals in the Stage II veins commonly show a schistose fabric, with the quartz crystals elongated parallel to the vein walls. Stage III vein pyrite and arsenopyrite, being competent sulphide minerals, are commonly fractured and brecciated. Fractures in arsenopyrite are locally filled by galena and gold. Galena, well known as a ductile sulphide mineral, readily migrates to low-pressure sites. Vein quartz shows local development of cataclastic and mortar textures with broken quartz fragments in a matrix of fine-grained recrystallised quartz. Quartz pressure shadows are formed around larger arsenopyrite crystals, indicating that the latter are pre- or syntectonic. Quartz in veins commonly shows undulose extinction, deformation bands and deformation lamellae.

Results

Whole-rock geochemical analyses

Average values are listed in Table 1 and concentrations of selected elements from one drill hole are plotted in Fig. 6. The average Au concentration in the samples from the four drill holes is about 2 ppm and is almost continuous at that level across the dyke (Fig. 6, Table 1). Gold values of up to 0.82 ppm were recorded in the lamprophyre (drill hole SC45), but Au values are typically less than 0.2 ppm in samples containing lamprophyre. Arsenopyrite–pyrite veins are absent from the metapelite and metasandstone country rocks, which contain no gold (limits of determination were 0.01 ppm; Table 1). Silver concentrations of drill core are variable, with an average grade of about 1 ppm, but can be as high as 35 ppm. Only As is strongly correlated with Au ($R^2 = 0.75$; Table 2), although in polished thin sections gold (2–100 μm in size) is often associated with galena as inclusions in arsenopyrite and pyrite crystals (Fig. 5B). Silver strongly correlates with Cu ($R^2 = 0.81$), but the reason for this is not clear. The average concentrations of Cu, Mo, and Bi are low ($<<$ 20 ppm), with average Cu concentrations higher in the metapelites (25 ppm) than the mineralised granite (16 ppm, Fig. 6). The average concentrations of As (~ 7,000 ppm), Zn (~325 ppm) and Pb (~150 ppm) reflect the predominance of arsenopyrite, with minor sphalerite and galena in the sulphide–gold veins.

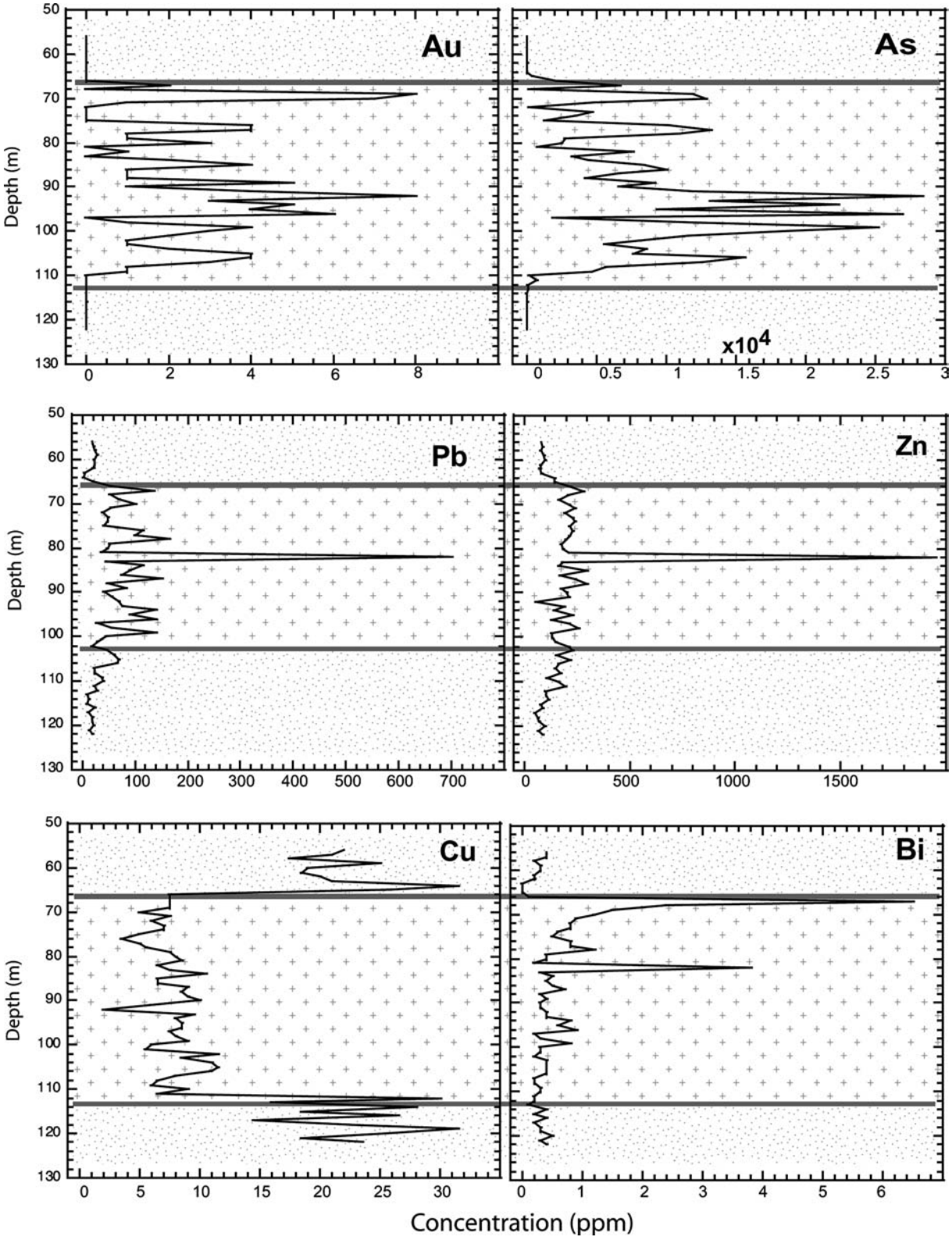

Fig. 6 Assay results (ppm) versus depth for drillhole SC45. One-metre long drillcore samples were analysed and results are plotted for Au, As, Cu, Pb, Zn and Bi. Data provided by Oceana Gold Ltd. *Dots* = Wangapeka Formation metapelite; *crosses* = Sams Creek granite

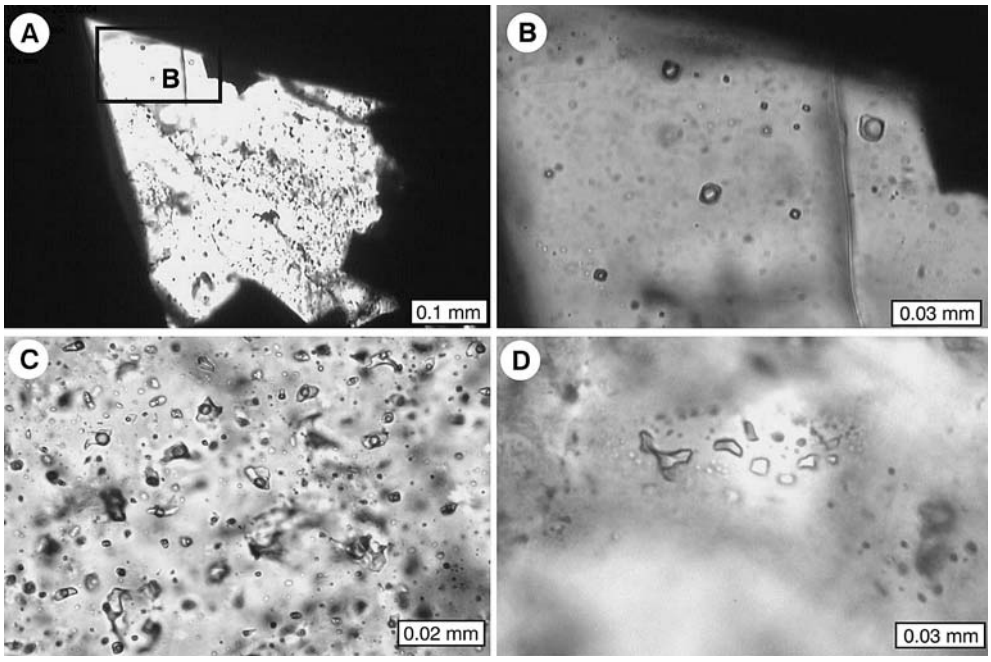

Fig. 7 Fluid inclusions in vein quartz. **a** Primary inclusions in quartz protected by arsenopyrite (apy). **b**. Enlargement of part of (A) showing two-phase carbonic liquid (dominant phase) + aqueous liquid inclusions. **c** Early secondary aqueous liquid-rich inclusions with variable vapour to liquid ratios preserved in quartz phenocryst in granite. **d** Secondary healed monophase inclusions. Photomicrographs in plane transmitted light

Mineral chemistry

Carbonates

Carbonate minerals are present in the Stage III veins and as alteration minerals in the granite and lamprophyre. The carbonate minerals analysed are mainly siderite, with ankerite restricted to lamprophyre samples (Table 3). This presumably reflects the higher magnesium and calcium contents of the lamprophyre compared to the granite. The EPMA oxide analyses have been recalculated as carbonates in Table 3. Some of the siderite samples also contain significant manganese (up to 4.6 wt% $MnCO_3$). A few of the siderites contain magnesium with up to 29.3 wt% $MgCO_3$, but most have over 80 wt% $FeCO_3$. The composition of the carbonate in the veins is similar to that in adjacent altered granite.

Gold

Gold analyses (Table 4) show a range in silver content from 15.8 to 30.0 wt% (average Au = 76.9 wt%), consistent with microscopic observations of colour variations from deep to pale yellow. Gold with >20 wt% Ag is more accurately termed electrum. Within individual samples the composition of the gold appears to be fairly uniform and is unrelated to the adjacent sulphide minerals; i.e. gold enclosed in galena is no more silver-rich than gold enclosed in arsenopyrite. Trace elements (Bi, Cu, and Sb) analysed for by EPMA are below their detection limits (0.1 wt%), except bismuth, which ranges from 0.4 to 1.1 wt%.

Fluid inclusions and microthermometry

Fluid inclusion microthermometry was carried out using Fluid Inc. and Linkam heating-freezing stages that were calibrated using synthetic fluid inclusions at −56.6°C, 0°C, and 374°C. Precision is estimated at ±0.2°C for freezing runs and ±2°C for heating to higher temperatures. The vein quartz at Sams Creek is extensively recrystallised and typically contains clouds of tiny, single-phase fluid inclusions (<2 μm in size) in planar arrays. Relict, possible primary fluid inclusions are rare and are preserved in clear quartz grains within and adjacent to arsenopyrite veins in the Main Zone (Fig. 7a, b). The rigidity of the arsenopyrite appears to have protected the quartz grains and their contained fluid inclusions from recrystallisation (cf. Marsh et al. 2003). The occurrence of these inclusions in three-dimensional patterns within individual quartz grains is the main criterion for their primary origin (cf. Roedder 1984). However, because of possible postentrapment modification, despite their apparent protection by the arsenopyrite host, it is misleading to call them primary (Marshall et al. 2000, and references therein) and they are referred to as "early formed" in this paper. Early-formed fluid inclusions are also locally preserved in unrecrystallised quartz phenocrysts in the granite (Fig. 7c). At room temperature, the early-formed inclusions occur as small (<10 μm), two- and three-phase carbonic liquid-rich inclusions containing liquid CO_2-CH_4 + liquid H_2O ± CO_2 vapour ($L_1 + L_2 \pm V$), and two-phase aqueous liquid-rich ($L + V$) inclusions. The $L + V$ inclusions are classified into those with clathrates ($L_{clath} + V$) and without clathrates ($L + V$). Within individual samples, the two- and three-phase carbonic liquid-rich inclusions do not coexist with the aqueous liquid-rich inclusions.

Remnants of other early fluid inclusions occur in deformed vein quartz as decrepitated fluid inclusions and as healed monophase inclusions (Fig. 7d). These remnant fluid inclusion morphologies are similar to those described from a metamorphosed ore deposit by Giles and Marshall (1994). The healed inclusions were interpreted by these authors as leaked inclusions which re-equilibrated to a lower bulk density under conditions of high-internal overpressure during rapid decompressive regional uplift. Some of the carbonic liquid-rich inclusions in quartz crystals that are not enclosed by arsenopyrite show variable degrees of fill, which suggests either trapping of a heterogeneous fluid or leakage during postentrapment modification. In some of these inclusions, leakage is consistent with the presence of some dark coloured, i.e. empty inclusions.

A previous study by Windle and Craw (1991) described CO_2-rich inclusions from the western part of the dyke (Western Outcrops and Riordans; Fig. 2), which coexisted with aqueous liquid-rich inclusions. They were interpreted to represent trapping of immiscible carbonic-rich and aqueous liquid at temperatures of 260–340°C. The Tm_{CO_2} (−56.6 to −58.1°C) indicates that the carbonic phase was mainly CO_2. Salinities estimated from ice melting and clathrate melting temperatures were in the range of 0 to 7.5 wt% NaCl equiv.

Microthermometric results

The carbonic liquid-rich $L_1 + L_2 \pm V$ inclusions in quartz adjacent to arsenopyrite homogenised by disappearance of the H_2O-rich liquid phase to vapour at temperatures of 320 to 354°C (Table 5). The $L_1 + L_2$ inclusions (Fig. 7b) contain water (L1) plus a pale brownish grey carbonic liquid (L2) which forms a vapour bubble on cooling to about −10°C. The vapour bubble homogenised to liquid at temperatures of −3.0 to +11.0°C. During freezing runs on these two-phase inclusions, the carbonic phase melted (Tm_{CO_2}) at temperatures of −63.5 to −62.0°C and a clathrate phase melted (Tm_{clath}) at 11.5 to 12.5°C. The three-phase inclusions ($L_1 + L_2 + V$) contain liquid water (L_1) plus carbonic liquid (L_2) and carbonic vapour (V) at room temperature. In these inclusions, the vapour bubble homogenised to liquid at temperatures of 20 to 26.7°C and the carbonic phase melted (Tm_{CO_2}) at a temperature of −62.0 to −66.3°C. These data suggest that the carbonic phase contains a significant component of other gases such as CH_4 and N_2 in addition to CO_2, because Tm_{CO_2} is well below the −56.6°C triple point of pure CO_2 (e.g. Diamond 2003). Using the curves of Thiéry et al. (1994) for the CO_2-CH_4 and CO_2-N_2 systems, none of the microthermometric data are consistent with the CO_2-N_2 system but some of the data are consistent with the CO_2-CH_4 system. The mole fraction of CH_4 in the carbonic phase, for one of the carbonic fluid inclusions (Tm_{CO_2} of −62.5°C and Th_{CO_2} of −3°C), is estimated at 0.25 from the VX diagram for the CO_2-CH_4 system at low-molar volumes of Thiéry et al. (1994). The presence of CH_4 in the fluid is consistent with the occurrence of graphite in the mineralisation.

The presence in individual quartz crystals of fluid inclusions containing only carbonic liquid and H_2O indicates trapping of a homogeneous fluid that separated into two immiscible liquids at the homogenisation temperatures of 320–355°C, rather than trapping of an immiscible two-phase assemblage. Therefore, these inclusions represent trapping of a single-phase fluid at temperatures (Tt) greater than Th (cf. Shepherd et al. 1985).

The aqueous liquid-rich inclusions containing clathrates ($L_{clath} + V$), have temperatures of homogenisation (Th) from 258 to 310°C and clathrate melting temperatures (Tm_{clath}) in the range 9.0 to 11.6°C. Liquid CO_2 was observed in one inclusion and a T_mCO_2 value of −57.6°C indicates near pure CO_2 in the carbonic phase. The ice melting temperatures (Tm_{ice}) of −1.0 to −3.8°C convert to apparent salinities of 1.7 to 6.2 wt% NaCl equiv. However, the presence of clathrates suggests that the higher values may be overestimates (Collins 1979).

The aqueous L + V inclusions without clathrates have $Th_{V\text{-}L}$ values in the range 185–305°C, with T_{mice} of −0.8 to −4.8°C. The higher part of the range of Th and the

Table 5 Summary of microthermometric data from fluid inclusions in vein quartz and quartz phenocrysts, Sams Creek gold deposit. Mode of homogenisation recorded as L, to liquid: V, to vapour. Degree of fill is the volumetric proportion of the aqueous H_2O-rich phase estimated visually at 25°C from charts of Shepherd et al. (1985). (9) = number of inclusions measured

Inclusion type	Carbonic liquid-rich $L_1 + L_2 \pm V$	Aqueous liquid-rich with clathrate $L_{clath} + V$	Aqueous liquid-rich L + V
Tm_{CO2}	−62.0 to −66.0 (9)	−57.6 (1)	
Th_{CO2}	−3.0 to 26.7 (7)	10.5 (1)	
Mode	L	L	
Tm_{clath}	9.0 to 12.5 (3)	9.0 to 11.6 (6)	
Tm_{ice}		−1 to −3.8 (4)	−0.8 to −4.8 (7)
Th	320 to 354 (10)	258 to 310 (14)	185 to 305 (11)
Mode	V	L	L
Th Mean	337	285	280
Salinity (wt% NaCl equiv)		1.7 to 6.2	1.4 to 7.6
Degree of fill	0.3–0.8	0.7–0.8	0.6–0.8

Table 6 Oxygen isotope values of vein quartz (qtz) and albite (alb), granite quartz and feldspar (fsp) phenocrysts (pheno). In some veins more than one quartz sample was analysed and for the granite duplicate/triplicate quartz and feldspar phenocrysts were analysed where possible. Veins have been identified as either Stage II or III, based on their relative timing and mineralogy. $\delta^{18}O_{magma}$ values (in brackets) are calculated from quartz and amphibole phenocrysts (see text)

	$\delta^{18}O$ ‰ (SMOW)				
	Stage	Vein qtz (alb)	Pheno qtz ($\delta^{18}O_{magma}$)	Pheno fsp	Amphibole ($\delta^{18}O_{magma}$)
SC1-4.5	II	15.4; 15.4			
SC15-18.1	III	15.9; 15.7			
SC15-21.7	III	15.7; 16.0			
SC16 4.7	II	12.0			
SC16 9.9	III	15.8			
SC16A 15.0	III	16.0; 16.1			
SC16A 20.9	II	14.4			
SC16A 26.2	II	14.7; 14.8			
SC17A-10.2	III	15.7; 15.8			
SC18-13.6	II	15.3			
SC25-160.0	III	16.1			
SC26-123.3	II	14.4			
SC29-29.8	III	16.3			
SC29 45.8	III	15.9; 15.7			
SC29 46.1	III	16.3			
SC29-56.5	III	15.6			
SC29 118.3	II	14.0; 14.2			
SC29 120.5	II	14.9			
SC32 16.8	III	16.1			
SC37 94.4	III	16.0			
SC37 88.5	III	16.1; 16.0			
SC38 4.6	III	16.3			
SC38 7.2	II	15.1 (13.0)	9.1; 8.9 (8.0)		
SC38 7.6	III	16.8			
SC38 7.6	II		8.8; 8.8 (7.8)		
SC38 31.1	III	16.2			
SC39 39.2	II		7.5; 7.2 (6.3)	6.6; 6.5	
SC39 47.6	III	16.7			
SC40 142.9	II	14.7; 14.7			
SC40 138.2	II	13.7			
SC40 95.9	II	14.8; 14.8			
SC40 105.5	II	14.7			
SC40 151.6				12.0	
SC40 152.3			7.7; 7.8 (6.8)	7.9; 7.7; 7.5	
SC42 199.5			7.5; 7.4 (6.4)	11.4; 11.7	
SC42 216.7			7.8; 7.7 (6.8)	11.6; 11.0	
SC42 246.8	II	14.8			
SC43 61.5				11.7; 12.0	
SC43 62.1			8.0; 8.2 (7.2)	9.3; 10.5	
SC46 105.5	II	14.5			
140103-2			7.6; 7.6 (6.6)	6.1; 6.2	5.7 (6.5)
P43154			5.9; 5.9 (4.9)	0.7; 1.0; 0.5	
P689136			6.1 (5.1)	8.5; 7.6	
P689114a			6.4; 6.2; 6.5 (5.4)	8.6	
P689114			6.5; 6.4 (5.5)		

apparent salinities of 1.4 to 7.6 wt% NaCl equiv overlap with the $L_{clath} + V$ inclusions, which suggests that they are of the same generation. Clathrate melting behaviour was not observed in these inclusions, but it may have been missed because of their small size.

Although, the Th values of early-formed fluid inclusions may only be minimum trapping temperatures and are suspect because of possible leakage, they are not too different from temperatures of 340–380°C obtained from stable isotope geothermometry (see below), suggesting that postentrapment modification of these selected inclusions may have been limited.

Stable isotopes

Quartz and feldspar phenocrysts from the Sams Creek porphyry granite have $\delta^{18}O$ values that range from +5.9 to +9.1‰ and 0.7 to +12.0‰, respectively (Table 6; Figs. 8, 9). In determining quartz phenocryst $\delta^{18}O$ values, care was taken to sample quartz phenocrysts that did not appear to be recrystallised (see "Sample Description" section). Quartz phenocrysts have similar $\delta^{18}O$ values and show good replication, regardless of whether samples had altered groundmass and feldspar phenocrysts or not. Feldspar phenocrysts on the other

hand had a wide range of values and poor replication, even though the feldspar appears visually to be unaltered (Table 6). One sample of amphibole was analysed from an unaltered granite sample and had a $\delta^{18}O$ value of $+5.7‰$.

The $\delta^{18}O$ values of quartz from veins in the Sams Creek granite range from $+12.0$ to $+16.8‰$, but have a bimodal distribution with modes at $+14.5$ and $+16‰$ that correspond to Stage II and Stage III mineralisation, respectively (Fig. 10). One vein (Stage II) has coexisting quartz and albite with $\delta^{18}O$ values of $+15.1$ and $+13.0‰$, respectively. The albite is unaltered, based on thin-section observations and XRD analysis. The $\delta^{18}O$ values of the vein siderite and ankerite in lamprophyre range from $+12$ to $+16‰$ and $\delta^{13}C$ values have an average of $-4.7‰$ ($1\sigma = 0.5‰$; Table 7; Fig. 11). Two siderite vein samples that have been severely brecciated (and most likely isotopically re-equilibrated) have $\delta^{18}O$ values that are outliers at about $+19‰$, but $\delta^{13}C$ values are unchanged. Bulk oxygen and carbon from the Wangapeka Formation metapelite adjacent to the Sams Creek granite and lamprophyre, has $\delta^{18}O$ and $\delta^{13}C$ values that range from $+13.6$ to $+16.0‰$, and -23.8 to $-19.3‰$, respectively (Table 7). The $\delta^{34}S$ values of the sulphides in veins in the Sams Creek granite range from $+5.0$ to $+9.9‰$, but have a bimodal distribution with modes at c. $+6‰$ and c. $+9‰$ which correlate with Stage II and Stage III mineralisation, respectively (Table 8; Fig. 12). A pyrite-rich sample from the Devil River Volcanics has a $\delta^{34}S$ value of $0.1‰$. The metapelites of the Wangapeka Formation contain pyrite blebs and bedded stringers with values that range from -3.5 to $+9.3‰$; most values are $< +4‰$ (Fig. 12). The Arthur Marble locally contains minor amounts of pyrite, which has values that range from $+3.6$ and $+13.1‰$.

Discussion

Granite source and alteration–oxygen isotope evidence

The whole-rock $\delta^{18}O$ value of an unaltered granite is diagnostic of the source of the magma (O'Neil and Chappell 1977). However, feldspars are susceptible to the effects of alteration and because the granite often consists predominantly of feldspar, the whole-rock method of estimating the $\delta^{18}O$ value of the magma ($\delta^{18}O_{magma}$) is not always reliable. Quartz on the other hand is much more resistant to alteration and its oxygen isotope value provides an alternative way to estimate the $\delta^{18}O_{magma}$ (Javoy and Weis 1987). The $\delta^{18}O$ value of quartz in a granite is dependent on the isotope fractionation between quartz and the melt ($\Delta_{quartz\text{-}magma}$) and also the cooling rate, which is reflected in the grain-size, and the temperature of closure of the quartz to oxygen diffusion (e.g. Giletti 1986). To correct for the "closure" effects, $\Delta_{quartz\text{-}magma}$ for quartz phenocrysts (fine-grained groundmass) are considered to be approximately $+1‰$ (Giletti 1986; Taylor and Sheppard 1986). Amphibole and pyroxene crystallise early in granites and do not equilibrate to lower temperatures like quartz; they are therefore also useful for estimating $\delta^{18}O_{magma}$ values. The $\Delta_{pyroxene/amphibole\text{-}magma}$ is $-0.8‰$ (Taylor and Sheppard 1986).

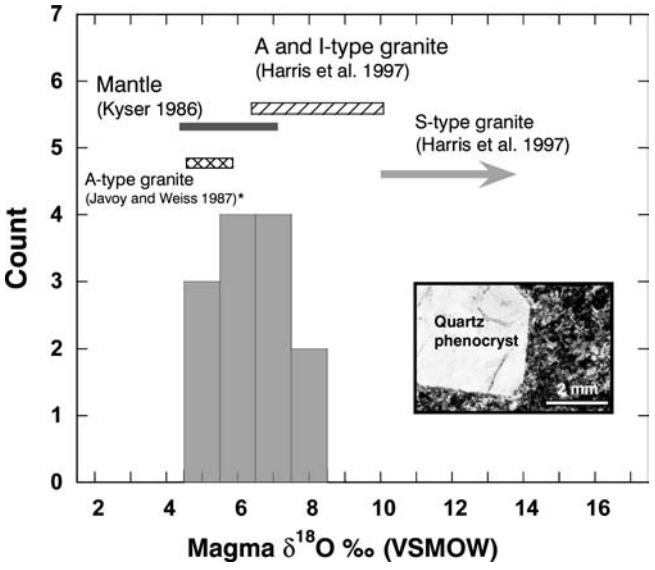

Fig. 8 Stacked histogram of calculated $\delta^{18}O_{magma}$ values (from quartz and amphibole phenocrysts –see text) for Sams Creek granite compared to those of other A-, I- and S-type granites and $\delta^{18}O$ values assumed for the mantle (bin size $0.5‰$). The A-type values from Javoy and Weiss (1987) have been corrected for "closure effects", assuming a $\Delta_{quartz\text{-}magma} = 1‰$. The inset photomicrograph (crosspolarised light) is an example of a quartz phenocryst, unaffected by hydrothermal alteration

The calculated $\delta^{18}O_{magma}$ values ($+5$ to $+8‰$) from Sams Creek granite quartz phenocrysts and one amphibole phenocryst ($+6.5‰$) overlap with those of other A and I type-granites elsewhere (Table 6; Fig. 8). This is consistent with the Sams Creek granite being an A-type granite, based on its major and trace element whole-rock geochemistry (Tulloch 1992). In his review paper on the isotope variations in the mantle, Kyser (1986) proposed that the mantle has $\delta^{18}O$ values that range from $+5$ and $+7‰$. In support of this, Javoy and Weis (1987) considered the $\delta^{18}O_{qtz}$ values ($+6.0$ to $+7.3‰$, not corrected for "closure" effects) from alkaline A-type granites to be consistent with a mantle origin. However, not all A-type granites have $\delta^{18}O$ values entirely of mantle origin. For example, the anorogenic complexes of Damaraland, Namibia, have $\delta^{18}O_{magma}$ values from $+4.9$ to $+12.0‰$, with values $>10‰$ reflecting a large crustal contribution (Harris 1995). In their study of the Cape Granite suite in South Africa, Harris et al. (1997) proposed that A- and I-type granites had $\delta^{18}O_{magma}$ values from $+6.6$ to $+9.9‰$ and were distinct from values obtained from S-type granites ($+9.5$ to $+11.4‰$; Fig. 8). The petrogenesis of A-type granites has been extensively studied, but remains a subject of debate and cannot be discussed in any detail

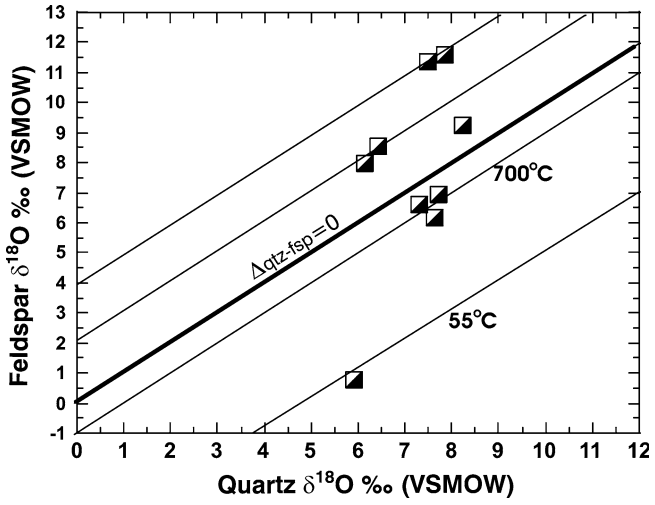

Fig. 9 Plot of $\delta^{18}O_{quartz}$ versus. $\delta^{18}O_{feldspar}$ values of phenocrysts from the Sams Creek granite on an "isotherm" plot (*solid lines* of equal temperature; Δ qtz-fsp = −1 corresponds to isotherm 700°C). Three samples appear to be in closed system isotope equilibrium indicating isotope closure temperatures of about 700°C. Samples above Δ qtz-fsp = 0 are definitely out of isotope equilibrium, as $\delta^{18}O_{quartz}$ is always > than $\delta^{18}O_{feldspar}$ when in isotopic equilibrium (see text for details)

here. Some workers have suggested that A-type granites are generated through partial melting of the lower crust (e.g. Collins et al. 1982). Others have postulated that there are genetic links between mantle-derived melts and A-type granites (e.g. Turner et al. 1992). A-type magmas have the potential to rise to very shallow levels in the crust (Whalen et al. 1987), possibly via temporary storage chambers near the brittle-ductile transition, and then breach the surface to form rhyolite or become trapped within the crust to form granite in extensional rift zones (Hogan and Gilbert 1995). Generally, A-type melts have occurred world wide throughout geological time in a variety of tectonic settings and do not necessarily indicate an anorogenic or rifting environment (e.g. Whalen et al. 1987). Nevertheless, the oxygen isotope data from Sams Creek quartz and amphibole phenocrysts are consistent with a relatively primitive, either mantle or mantle-derived crust, source for the granite magma with little or no evolved crustal input.

If minerals such as quartz and feldspar in a granite were in isotopic equilibrium they would plot on a straight line with slope 1 on a $\delta^{18}O_{feldspar}$ versus $\delta^{18}O_{quartz}$ plot (δ-space). When a fluid is brought into contact with the granite, postcrystallisation, the relative rates of exchange between the individual minerals and the fluid are highly variable and this is reflected in variable $\Delta\ ^{18}O_{quartz\text{-}feldspar}$ values and positive-sloped disequilibrium arrays in δ-space (Gregory et al. 1989). In the case of the Sams Creek quartz and feldspar phenocrysts, the data plot in a positive-sloped disequilibrium array (Fig. 9). Some of the data have $\Delta\ ^{18}O_{quartz\text{-}feldspar}$ of about 1‰ which correspond to oxygen isotope equilibrium temperatures of about 700°C, which could represent isotope equilibrium conditions, or may be fortuitous given the range of feldspar values. Samples with negative $\Delta\ ^{18}O_{quartz\text{-}feldspar}$ values (those that plot above the $\Delta\ ^{18}O_{quartz\text{-}feldspar} = 0$ line) cannot represent equilibrium temperatures under any condition. Even samples (P43154, P68913, and P68914a; Table 6) which do not appear to have any apparent signs of feldspar alteration, are not in isotope equilibrium. The relatively high $\delta^{18}O_{feldspar}$ values may be due to isotope exchange with isotopically heavy fluid such as magmatic water (i.e. deuteric alteration) or a meteoric water that has undergone extensive isotopic exchange with isotopically heavy country rocks during circulation at high temperatures (> 500°C), or due to isotope exchange with isotopically light meteoric water at low temperatures (< 200°C; e.g. Criss et al. 1984). This temperature is substantially lower than the fluid inclusion homogenisation temperatures from vein quartz (320 to 355°C), but the granite samples are generally distant from the main alteration/mineralisation and could reflect regional lower greenschist deformation or distal hydrothermal alteration. One sample has feldspar with a very low $\delta^{18}O$ value (c. +1‰), indicating isotopic exchange with an isotopically light water (e.g. meteoric) at relatively elevated temperatures (> 300°C).

O, C and S isotope values of vein and alteration minerals

Quartz

Mineralogical studies have shown that if quartz has been recrystallised, the $\delta^{18}O_{quartz}$ values could be partially or completely re-equilibrated, depending on the extent and temperature of recrystallisation (Voll 1976; Kerrich

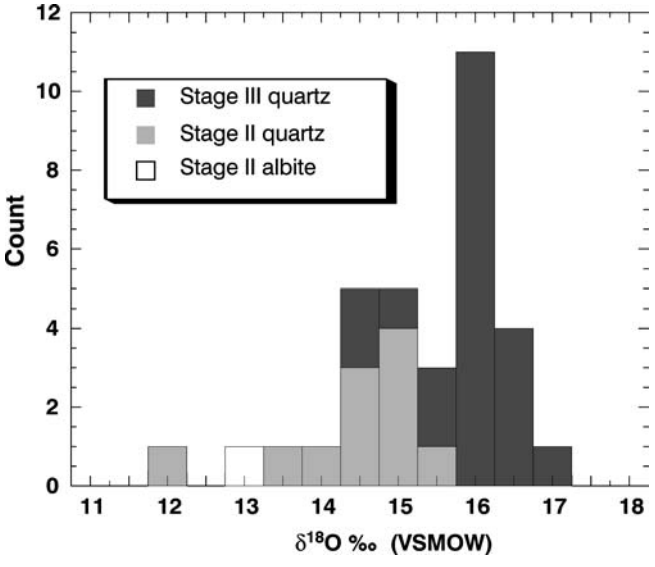

Fig. 10 Stacked histogram of $\delta^{18}O$ values of vein quartz and one sample of albite from a vein (bin size 0.25‰). Stage II quartz veins have lower values than Stage III quartz veins

et al. 1977; O'Hara et al. 1997). O'Hara et al. (1997) proposed that the onset for dynamic recrystallisation of quartz in deformation zones commences at temperatures of about 350°C. At Sams Creek, the regional lower greenschist facies metamorphic grade and relatively high $\delta^{18}O$ values of the granite feldspar phenocrysts, suggest that metamorphic temperatures were generally lower than 300°C. Hand specimen and thin section inspection clearly indicate that most of the quartz veins have undergone brittle and shear deformation and have been recrystallised to varying degrees. However, relict unrecrystallised grains are still present in this low-temperature/high-strain rate regime (cf. O'Hara et al. 1997). The $\delta^{18}O$ values of some of the vein quartz analysed may have been partially re-equilibrated. However, the small differences in $\delta^{18}O_{quartz}$ values from the same vein, the apparent preservation of isotopic equilibrium in one vein that contained quartz and albite (SC38-7.2; Table 6), and the preservation of the bimodal distribution of values associated with different mineralisation stages, suggests that values have not been changed significantly by the deformation. Also the $\delta^{18}O$ values of phenocryst and vein quartz are very different (by $\sim 8‰$). If these had been significantly affected by either regional or local recrystallisation, the differences would not have been preserved.

Table 7 Carbon and oxygen isotope results for Sams Creek vein siderite and ankerite[a] in granite and lamprophyre[b], and bulk carbon[c] and oxygen[d] from the Wangapeka Formation. Numbers in brackets are the weight % carbon measured in sample

	$\delta^{13}C$ ‰ (VPDB)	$\delta^{18}O$ ‰ VSMOW
SC19 226.8[a]	−4.9	14.1
SC25 144.2	−5.1	14.1
SC25 151.7	−4.8	13.9
SC25 159.1	−5.2	14.0
SC25 176	−5.5	14.4
SC25 171.1	−4.4	16.0
SC25 176.4	−4.3	14.0
SC29 120.9[d]		15.1
SC29 121.0[c] (0.86)	−22.1	
SC39 54.7	−4.9	14.6
SC 39 54.7	−5.0	14.1
SC40 104	−4.1	12.2
SC40 108.9[d]		13.6
SC40 121.6	−4.7	14.1
SC 40 154.3[b]	−4.4	13.5
SC 40 154.4[a]	−4.3	13.9
SC 42 195.5	−4.9	13.8
SC 42 223.1	−4.5	19.8
SC42 256.4	−4.7	14.0
SC43 11.4[c] (0.56)	−23.8	
SC 43 46.0	−5.7	14.1
SC 43 73.8	−4.6	14.9
SC 43 113.3[d]		16.0
SC43 121.8[c] (0.86)	−19.3	
SC44 173.1	−4.4	13.2
SC44 173.2	−4.3	13.6
SC44 276.2	−4.1	14.4
SC44 327.0[d]		15.8
SC45 67.3	−4.0	19.5
SC45 67.3	−5.0	15.0
SC45 67.3	−5.0	15.0
SC48 190.2	−4.4	14.3
SC48 222.0	−4.2	14.4
SC48 221.3	−4.9	12.6

The reason for the bimodal $\delta^{18}O_{quartz}$ values may be that Stage II veins were formed from fluids with relatively lower $\delta^{18}O_{H_2O}$ values or slightly higher temperatures, or a combination of the two, compared with Stage III veins. One vein from Stage II contained quartz ($\delta^{18}O$ values = 15.1‰) and albite ($\delta^{18}O$ values = 13.0‰), giving a $\Delta_{quartz\text{-}albite}$ value of 2.1‰. Assuming isotopic equilibrium between the minerals, the calculated temperatures of 340°C (fractionation factors of Zheng 1993) and 380°C (fractionation factors of Clayton and Kieffer 1991) are not too different from temperatures (300 to 365°C) indicated for Stage III veins from fluid inclusion Th measurements. If the $\delta^{18}O_{H_2O}$ values were the same for Stage II and Stage III veins, then Stage II veins formed at approximately 50°C higher than Stage III veins, using the Clayton et al. (1972) fractionation factors.

Assuming temperatures of vein formation between 300 and 360°C and the total range of $\delta^{18}O$ values of vein quartz (+12 to +17‰), the calculated $\delta^{18}O_{H_2O}$ values range from +6 to +12‰. If an average temperature of 340°C and the $\delta^{18}O$ mode values (+14.5 and +16‰) are used, then the calculated $\delta^{18}O_{H_2O}$ values are 8 and 10‰ for Stage II and Stage III mineralisation, respectively (fractionation factor of Clayton et al. 1972). These values overlap with those of magmatic origin or water equilibrated at high temperature with magmatic rocks (+5 to +10‰), but also with those considered to be of metamorphic origin (+5 to +20‰; Sheppard 1986). Windle and Craw (1991) suggested that the hydrothermal fluid was of metamorphic origin. Assuming that the premetamorphic $\delta^{18}O_{WR}$ values of the Wangapeka Formation were similar to the postmetamorphic values (~15‰, Table 7), the metamorphic fluids would have had $\delta^{18}O_{H_2O}$ values range from +12 and +15‰ (Zheng 1993, albite-water fractionation factor at 500°C). Quartz precipitating at 350°C from these fluids would have had values of about +19‰ (Zheng 1993), higher than the total range of the Sams Creek vein quartz (+12 to +17‰). Based on oxygen isotope results, therefore, the Wangapeka Formation does not appear to be the source of the hydrothermal fluids, although a deeper source cannot be ruled out.

Carbonate

Siderite in veins at Sams Creek have $\delta^{18}O$ and $\delta^{13}C$ values in a relatively narrow ranges (+14‰, ±2‰), and −4.7‰, ±0.5‰, respectively; Fig. 11). The $^{18}O/^{16}O$ ratios of siderite are much more sensitive to temperature of formation than $^{13}C/^{12}C$ ratios, but the latter are good tracers for the source of fluids. Thus, values for siderite point towards a large, well-mixed oxygen and carbon isotope reservoir and constant physico-chemical conditions during precipitation.

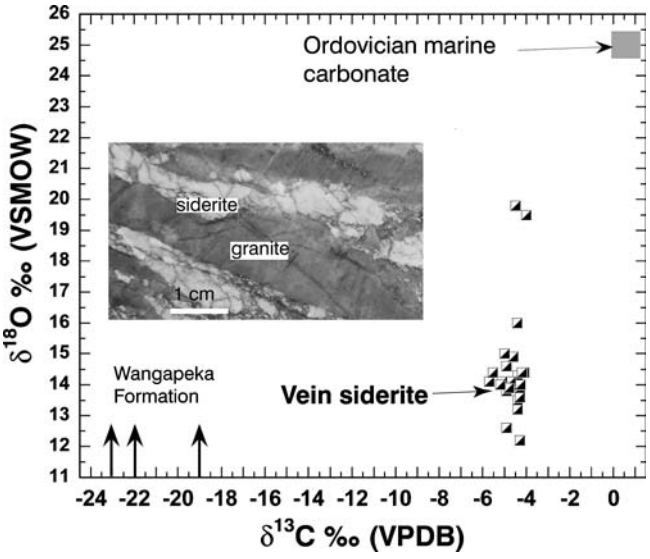

Fig. 11 $\delta^{18}O$ versus $\delta^{13}C$ values for siderite in Sams Creek granite and ankerite in lamprophyre. Also shown are the $\delta^{13}C$ values of bulk carbon obtained from the Wangapeka Formation and Ordovician marine limestones (Veizer et al. 1999). Inset photo: Siderite veinlet in Sams Creek granite

Recent determination of $^{18}O/^{16}O$ fractionation between siderite and water (45 to 75°C) by Zhang et al. (2001) has confirmed the fractionation results of Carothers et al. (1988) at low temperatures. In addition, the fractionations determined by Carothers extrapolated to higher temperatures (about 300°C), are in good agreement with those proposed by Zheng (1999). The exact temperature of formation for the Sams Creek siderite is not known, but assuming temperatures of 250 and 350°C, then calculated $\delta^{18}O_{H_2O}$ values for siderite (+12 to +16‰) range from +5 to +10‰ (fractionation factors of Carothers et al. 1988). These $\delta^{18}O_{H_2O}$ values are in agreement with those calculated from vein quartz and are in the range of magmatic-hydrothermal fluids (Sheppard 1986). The values are lower than calculated $\delta^{18}O$ values (between +12 and +15‰) of water from dehydrated Wangapeka Formation metapelite (see previous section), although water of deep metamorphic origin cannot be excluded.

Early formed fluid inclusions in vein quartz at Sams Creek indicate that carbon in the hydrothermal fluids was mainly dissolved as CO_2 (H_2CO_3), although some fluid inclusions contain up to 0.25 mole% CH_4. Many experimental studies show that isotopic exchange between gaseous species of the C-O-H system (particularly CH_4-CO_2) is very slow even at temperatures up to 500–600°C (Chacko et al. 2001). The carbon isotope equilibrium fractionation between CH_4-CO_2 at 300°C is about −25‰ (Richet et al. 1977) and partial (kinetic) equilibrium between these two gases is not consistent with the uniform values of −5‰ (average −4.7‰; 1σ error ± 0.5‰) obtained for the Sams Creek vein siderite. Isotope fractionation between CH_4-CO_2 is therefore assumed to be insignificant during the hydrothermal stages. The $^{13}C/^{12}C$ fractionation between siderite and CO_2 at 250 and 350°C is small (0 to 2‰; Carothers et al. 1988; Golyshev et al. 1981), and therefore a calculated $\delta^{13}C_{CO2}$ value for the hydrothermal fluids is considered to be close to −5‰.

CO_2 with $\delta^{13}C$ values of about −5‰ is consistent with, but not unique, to fluids of magmatic/mantle origin. Potential sources for carbon in the Sams Creek hydrothermal fluids include the Wangapeka Formation with bulk $\delta^{13}C$ values between −19 and −24‰ (Table 7), and the underlying Arthur Marble (Ordovician marine carbonates) with $\delta^{13}C$ and $\delta^{18}O$ values of 0 and +22‰ (Veizer et al. 1999), respectively (Fig. 11). The calculated $\delta^{13}C$ value of CO_2 generated by metamorphic decomposition (c. 400°C) of graphite in the Wangapeka Formation (about −22‰) would be approximately −12‰ (cf. Bottinga 1969) and, the CO_2 produced by thermal decarbonisation of Arthur Marble is expected to have a $\delta^{13}C$ value (c. 0‰) similar to that of carbonate (Ohmoto and Goldhaber 1997). It is possible that the carbon in the vein siderite consists of carbon released during metamorphic volatilisation reactions, with variable contributions from graphite in the Wangapeka Formation (~40%) and carbonate in the Arthur Marble (~60%). However, we have demonstrated on the basis of oxygen isotope values of the quartz and siderite veins, that neither of these formations are likely sources. In addition, the vein siderite has a remarkably low variation in $\delta^{13}C$ values throughout the deposit, with no indication of mixing between any of these carbon (and oxygen) isotope reservoirs.

The geochemical composition of the Sams Creek granite (Tulloch 1992) and calculated $\delta^{18}O_{magma}$ values in this study indicate a primitive origin, such as the mantle or mantle-derived crust. Carbon with $\delta^{13}C$ values of about −5‰ has been identified as an important isotope signature for the mantle (carbonatite and kimberlite carbonates, diamonds, and volcanic CO_2 exhalations) and is also observed in mantle xenoliths (Deines 2002, and references therein). The $\delta^{13}C_{CO_2}$ value of about −5‰ for the Sams Creek vein siderite is therefore consistent with a magmatic, possibly mantle or mantle-derived, source for ore-forming fluids. By itself, a $\delta^{13}C_{CO_2}$ value of about −5‰ is not unique to hydrothermal magmatic deposits (Ohmoto and Goldhaber 1977). However, carbonates from veins which have been interpreted to have formed from predominantly metamorphic fluids in the South Island at Macraes Flat Au deposit (Craw et al. 1995) and Benmore Dam (de Ronde et al. 2001), have $\delta^{13}C$ values that range from −10 to −13‰ and −25 to −38‰, respectively, consistent with fluids that have interacted with crustal rocks.

In summary, the Sams Creek carbon and oxygen isotope values of carbonates in veins are consistent with a magmatic, possibly mantle or mantle-derived crustal source for fluids and carbon in the deposit. Potential local source rocks outside the Sams Creek granite are not suitable candidates for fluid sources, although a deep crustal source cannot be ruled out.

Table 8 Sulphur isotopes results (‰, CDT) of sulphide minerals from Sams Creek veins, Wangapeka Formation[a], the Arthur Marble[b] and the volcanic Devil River Group[c]

	Stage	δ^{34}S py	δ^{34}S sl	δ^{34}S apy	δ^{34}S cp
SC1 8.0	III	9.1			
SC15 18.1	III	9.2			
SC15 21.7	III	9.2	5.0		
SC16 4.7	III	9.7		9.8	
SC16 9.9	III	9.5		9.7	
SC16A 15.0	III	9.9			
SC16A 20.9	III	9.8			
SC16A 26.2	III	9.3			
SC17A 10.2	III	9.5			
SC18 13.6	III	9.3			
SC22-6.0	III	8.2			
SC25 160	III		7.8		
SC25 174.8	III			9.1	
SC25 177.7	III			8.8	
SC29 46.1	II	5.5			
SC29 29.8	II	6.0		8.2	
SC36 10.7	II			9.0	
SC37 94.4	II	5.0			
SC37 95.5	II	6.7			
SC39 29.6	II	4.9			
SC39 31.1	II	5.1			
SC39 47.0	II	5.0			
SC40 117.0	III	9.5		8.6	
SC40 121.6	III	8.9			
SC42 195.0	III	8.5			
SC42 256.4	II	5.6			
SC43 12.0 [a]		−3.5; −2.6			
SC43 114.0 [a]		1.1; 2.1			
SC43 115.0 [a]		0.3; 1.1			
SC43 115.3 [a]		1.0; 0.7			
SC43 139.0	III			8.6	
SC44 136.5 [a]		3.4; 1.3			
SC44 251.6	III	8.1		8.4	
SC44 327.0 [a]	II	6.4			
SC45 92.0	III			8.4	
SC45 118.1 [a]		9.3			
SC48 206.8	III	7.7		8.4	
SC48 221.3	III	8.2		9.9	8.2
SC48 240.2 [a]		2.6			
CN652 [b]		6.7			
CN632 [b]		13.1			
CN1078 [b]		4.1			
CN 1079 [b]		3.6			
DevRivGrp[c]		0.1			

Abbreviations: *py* pyrite; *sl* sphalerite; *apy* arsenopyrite; *cp* chalcopyrite; *DevRivGrp* Devil River Group

Sulphides

Variation of δ^{34}S values of sulphide minerals and fluids may be caused by variation in temperature ($\Delta_{\text{mineral-fluid}}$), redox state, pH and the isotope value of the sources of the sulphur (Ohmoto 1972). In the case of Sams Creek the oxidation state of the hydrothermal fluids varied from high fO_2 (magnetite) in Stage I to low fO_2 in Stage III, based on the presence of pyrrhotite and graphite in veins, and CH_4 in some fluid inclusions. The dominant sulphur species in the Stage III fluid was therefore most likely H_2S and the following approximation may be used: $\delta^{34}S_{H_2S} \approx \delta^{34}S_{\text{sulphide mineral}}$ (Ohmoto and Goldhaber 1997).

Igneous rocks and associated ore deposits have a relatively wide range of δ^{34}S values (−10 to +15‰), depending mostly on the δ^{34}S values of sulphides or sulphates in country rocks (Ohmoto and Goldhaber 1997; Poulson et al. 1991; Ishihara et al. 2000). Sulphur is a sensitive indicator of degree of interaction between magma and any sulphur-bearing country rocks into which the magma is intruded, because sulphur is much more susceptible to mobilisation (due to the volatile nature of S) than other commonly used elements (REE, Rb/Sr, Sm/Nd and Pb; Poulson et al. 1991). The hydrothermal mineralisation and alteration at Sams Creek is confined to the granite and, to a lesser extent, the precursor lamprophyre which occurs between the granite and metapelite country rocks. This suggests that the mineralising fluids have not scavenged from, or lost, sulphur to the adjacent metasedimentary country rocks.

Sulphur isotope values of Sams Creek sulphide minerals range from +5 to +10‰ and, similar to the δ^{18}O values of the vein quartz, have a bimodal distribution (+6‰ and +9‰) associated with Stage II pyrite and Stage III sulphides, respectively (Fig. 12). Assuming a temperature of 350°C, based on the oxygen isotope results, calculated $\delta^{34}S_{H_2S}$ values for Stage II and III are approximately 5 and 8‰, respectively (using fractionation factors of Ohmoto and Goldhaber 1997). Therefore, the composition of the source of sulphur may have varied between the two stages. Another explanation is that the fluids had the same $\delta^{34}S_{H_2S}$ value, but that the pH of the fluid increased during the formation of Stage III sulphides. A pH increase from about 6 to 7.5 for a reduced fluid would increase the δ^{34}S value of sulphides by about 4‰ (Ohmoto 1972). However, there is no evidence from the mineralogy to verify an increase in pH from Stage II to Stage III veins. An increase in fO_2 of the hydrothermal fluid from stage II to III would also result in an increase in δ^{34}S of sulphides. Decreasing fO_2, as suggested by the mineralogy, would change the SO_2/H_2S ratio of the fluid towards H_2S dominance, so that the δ^{34}S of sulphides would increase to approximate the bulk S value. This would seem to be a simple and more likely explanation. In sample SC15-21.7 sphalerite (δ^{34}S value = +5‰) and pyrite (δ^{34}S value = +9.2‰) occur together in a vein and appear to be in textural equilibrium (Table 8). However, the $\Delta_{\text{py-sph}}$ = 4.2‰ equates to a temperature of −6°C, assuming isotopic equilibrium (Ohmoto and Goldhaber 1997), so sphalerite and pyrite in this sample are clearly not in isotopic equilibrium. Where they occur in the same sample, pyrite and arsenopyrite have similar values in most cases, suggesting that they are in isotopic equilibrium. No primary igneous sulphides were found in the Sams Creek granite or the lamprophyre to compare values to those obtained from sulphides associated with postmagmatic alteration/mineralisation.

A possible source of sulphur is the Wangapeka Formation metapelite which commonly contains pyrite blebs and bedded stringers. The δ^{34}S values of pyrite from the Wangapeka Formation range from −3.5 to

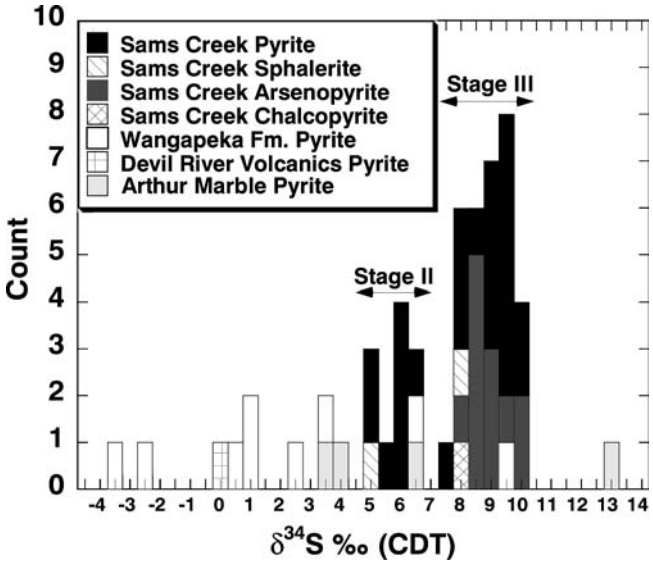

Fig. 12 Stacked histogram of δ^{34}S values obtained from sulphides in veins within the Sams Creek granite and values of pyrite sampled from the Wangapeka Formation, Arthur Marble and Devil River Volcanics Group (bin size 0.5‰)

+9.5‰, with most values less than +4‰ (Fig. 12). The δ^{34}S values of pyrite in the Wangapeka Formation are similar to those obtained from metasediments that host orogenic Au deposits in the Otago goldfields of New Zealand (range from −6 to +2‰; Craw et al. 1995). These values are in contrast to the δ^{34}S values from Sams Creek veins which have a relatively narrow range (5‰) and are generally higher.

Another possible source of sulphur is the Arthur Marble, which locally contains minor pyrite (0–3 wt%), with values ranging predominantly from +3 to +7‰ (one value at +13‰) that overlap with values obtained for Stage II veins (Fig. 12). Thus, the relatively high δ^{34}S values of Sams Creek sulphides are consistent with an enriched ^{34}S marine sulphur contribution. However, the δ^{13}C and particularly the δ^{18}O values of siderite and quartz in the Sams Creek veins are not consistent with this source (see above). In addition, the only samples from Arthur Marble that have trace amounts of pyrite are those that have been metamorphosed/altered (Roger Cooper, GNS Science personal communication 2005) and the δ^{34}S values of the pyrite may therefore reflect the alteration process, i.e. be derived from, not a source of, hydrothermal sulphur.

It is possible, but unlikely, that the Devil River Volcanic Group may be a source of sulphur for the Sams Creek sulphides. One sample analysed from a pyritic greenschist in this unit has a δ^{34}S value of 0‰. However, the spatial relationship between the Devil River Volcanic Group and the Wangapeka Formation/Sams Creek granite dyke at the time of mineralisation is uncertain, because of allocthonous contacts between the units (see Regional Setting).

Another possible source of the sulphur is from the mantle, or mantle-derived rocks. Analyses of sulphides in mantle-derived basalts and gabbros as well as from xenoliths in alkali basalts, kimberlites and diamonds yield δ34S values ranging from −11 to +14‰ (Schneider 1970; Chaussidon et al. 1987; Harmon et al. 1987; Eldridge et al. 1991; Ionov et al. 1992). Ionov et al. (1992) concluded that sulphides with largely positive δ^{34}S values predominate in the lithospheric mantle globally. Melts with positive δ^{34}S values can be generated from mantle peridotites with larger degrees of depletion and/or from rocks metasomatised by subduction-related fluids (Harmon and Hoefs 1986; Harmon et al. 1987; Chaussidon et al. 1987). In a study of magmatic-hydrothermal gold deposits related to granitoids, Ishihara and Sasaki (2002) and Ishihara and Murakami (2004) observed that sulphides in back-arc granitoids had relatively high δ^{34}S values (0 to +10‰). They proposed that the ore sulphur from these deposits had a deep, possibly upper mantle source, as a consequence of addition of seawater sulphate through subduction processes.

Overall, other than a continental mantle source, the only other likely source of sulphur for the sulphides in the Sams Creek mineralisation is the marine carbonates of Arthur Marble formation. However, we suggest that the latter possibility is unlikely, because oxygen and carbon isotope data of quartz and siderite in the veins are incompatible with a marine carbonate source. In addition, the source of the sulphur in the Arthur Marble carbonates may be hydrothermal. A mantle source for the sulphur from the Sams Creek Au deposit is consistent with other isotope evidence that some of the components associated with the granite and the hydrothermal fluids had a mantle or mantle-derived crustal source.

Comparison of Sams Creek with orogenic and intrusion-related Au-deposits

Similarities of Sams Creek with orogenic lode gold deposits include the low sulphidation state of the ore mineral assemblage (arsenopyrite and pyrite), carbonate alteration and carbonic fluid inclusions. However, there are also significant differences such as the high-sulphide content, significant amounts of galena, sphalerite and chalcopyrite, lack of scheelite or stibnite, early magnetite-siderite ± biotite alteration, and the relatively saline (up to 7.6 wt% NaCl equiv) fluid composition at Sams Creek. Additional differences from orogenic gold deposits are the stockwork-type veining and absence of mineralisation in the metapelite country rocks. Windle and Craw (1991) proposed that the Sams Creek deposit was of the "slate belt" (orogenic gold type) and contended that the mineralisation was confined to the granite because of its distinctive Fe^{3+}-rich composition. It is conceivable that the mineralisation could be syntectonic, but the lack of any through-going structural control on the veins and the gross relationship of the mineralisation and alteration to the granite host rock are

inconsistent with a syntectonic origin. The only known orogenic gold–quartz lodes in the region (Golden Blocks) are hosted in Ordovician metagreywackes and slates of the Buller Terrane Fig. 1.

The lack of definitive ages for the host granite porphyry and the mineralisation means that a conclusive genetic relationship between the granite and the alteration/mineralisation remains to be determined. Nevertheless, the Sams Creek gold deposit shows similarities with granite-related gold deposits of both the gold-rich porphyry-type deposits (Sillitoe 2000) and those related to ''reduced'' granitic intrusions (e.g. Thompson and Newberry 2000; Rowins 2000; Lang and Baker 2001). The stockwork-style sulphide–quartz veins and the presence of an early magnetite-bearing hydrothermal alteration assemblage are a feature of many gold-rich porphyry deposits. However, the high-SiO_2 and peralkaline composition of the Sams Creek granite, and the absence of molybdenite and paucity of chalcopyrite, are major points of difference. The presence of sericite–carbonate alteration and CO_2-rich fluid inclusions are typical of many of the ''reduced'' granitic intrusions types. However, some notable differences between the Sams Creek granite and the ''reduced'' granitic intrusions type are: (a) the Sams Creek granite is peralkaline whereas the reduced type are generally metaluminous and calc-alkaline and rarely alkaline; and (b) the Sams Creek deposit has high As only, and lacks the elevated Bi, W, Mo, Te, and/or Sb of the ''reduced'' type.

An association of gold-rich deposits with alkaline magmatism has also been recognised (e.g. Müller and Groves 1993; Richards 1995; Jensen and Barton 2000). The Sams Creek deposit shows some affinities with this group, although within this group granites with high SiO_2 are typically associated with Mo–Au mineralisation rather than the As–Au ± Pb–Zn mineralisation found at Sams Creek. No direct link can be made between the mineralisation and the lamprophyre at Sams Creek, except that it is a host rock. However, the close spatial relationship of the granite and lamprophyre dykes may be a manifestation of a similar geological setting, associated with an influx of mantle-derived magma, or heat that resulted in partial melts which were intruded into the Takaka Terrane (cf. Windle 1989;Wyman and Kerrich 1988, 1989).

As noted in many reviews, gold deposits associated with granitoids are a diverse group and the Sams Creek deposit, while showing some features of the various groups, appears to be a variant within this spectrum, as an As–Au deposit associated with a peralkaline granite (Brathwaite and Faure 2004).

Summary and conclusions

The Sams Creek granite, a peralkaline porphyry dyke ~40 m thick and about 7 km in length, intrudes Ordovician-Silurian metapelites, quartzites and marble. The granite also intrudes a lamprophyre (camptonite) which occurs as xenoliths in the granite and as thin dykes (0.2–3 m thick) between the granite and the metasedimentary rocks. Sulphide-gold-quartz-siderite veins and associated hydrothermal alteration are confined to the Sams Creek granite and to a lesser extent the lamprophyre. The metasedimentary rocks have undergone three phases of folding and the granite and lamprophyre dykes have been deformed and disrupted by the last two stages of folding. The age of the first phase of folding is middle Devonian, but the timing of the second phase (F_2) is uncertain. The third phase (F_3) is probably Early Cretaceous in age. The granite, lamprophyre, and sulphide–gold–quartz–siderite veins have been deformed and partially recrystallised.

$\delta^{18}O_{magma}$ values (+5 to +8‰) for the granite, calculated from quartz and amphibole phenocrysts, indicate a mantle, or reworked mantle-derived crustal source, which is consistent with the A-type granite classification of Tulloch (1992) based on major and trace element whole-rock geochemistry. Feldspar phenocrysts in the Sams Creek granite are generally not in oxygen isotope equilibrium with the quartz and reflect alteration by relatively ^{18}O-enriched fluids, such as deuteric fluids or fluids that have equilibrated with isotopically heavy country rocks at elevated temperatures (>500°C), or more likely, due to isotope exchange with isotopically light meteoric water at temperatures lower than 300°C.

Three stages of hydrothermal alteration and mineralisation have been identified in the granite. Stage I is characterised by high fO_2 magnetite–siderite ± biotite, Stage II by thin quartz–pyrite veinlets, and Stage III by low fO_2 sulphide, quartz and siderite veins, and pervasive silicification, represented by quartz–perthite–albite–rutile ± pyrite–siderite–sericite assemblages. The main stage of ore mineralisation is Stage III sulphide veins comprising arsenopyrite + pyrite ± galena ± sphalerite ± gold ± electrum ± chalcopyrite ± pyrrhotite ± rutile ± graphite deposited by H_2S-bearing, relatively saline, carbonic fluids. Deformation has resulted in partial fracturing and recrystallisation of vein quartz and sulphide minerals. Rare early-formed fluid inclusions are preserved in unrecrystallised quartz that was shielded by arsenopyrite and comprise carbonic two- or three-phase (liquid CO_2-CH_4 + liquid H_2O ± CO_2 vapour) inclusions, or two-phase liquid-rich aqueous inclusions. Final homogenisation temperatures (Th) of the carbonic inclusions indicate minimum trapping temperatures of 320 to 355°C. Quartz-albite stable isotope thermometry indicates temperatures of formation of 340 to 380°C, which are consistent with the fluid inclusion data. Mineralising fluids have calculated $\delta^{18}O_{water}$ values (from vein quartz and siderite) of about +8‰ (Stage II) and +10‰ (Stage III), calculated $\delta^{13}C_{CO_2}$ values of about −5‰ (from siderite) and $\delta^{34}S_{H_2S}$ values of about +5‰ (Stage II) and +8‰ (Stage III). A lack of definitive dating results means that a time correlation between granite emplacement and the alteration/mineralisation has not been definitely established. However, the close spatial relationship of the

granite and lamprophyre dykes and the mineralisation suggests that the hydrothermal fluids were sourced from crystallisation of the granite magma or an associated underlying magma chamber. Other potential sources for the hydrothermal fluids, such as metamorphic devolatilisation of the adjacent metapelites and the underlying Arthur Marble marine carbonates are not likely, although deeper sources cannot categorically be excluded. An overall view of the data, including the style of veining and the sulphide mineralogy, suggests that a magmatic source is more likely.

If this interpretation is correct, then Sams Creek appears to be a hybrid between intrusion-related gold deposits described as reduced granite Au–Bi deposits and alkaline Au–Mo–Cu intrusive hosted deposits.

Acknowledgements Oceana Gold Ltd (formerly GRD Macraes) provided access to drill core and information on the Sams Creek prospect. In particular we thank Lachlan Reynolds, Sean Doyle, Austin Osborne and Peter Grieve for their help. We acknowledge the help of Cornel de Ronde who provided the impetus to start our research on Sams Creek, and Andy Tulloch, Ian Graham, Roger Cooper and Richard Jongens for discussions. We thank Phil Warnes, Karyne Rogers, Ray Soong, Neville Orr, Steve Mawdesley, Christine Prior, Julia Vodanovich and John Simes for their technical assistance. The study was funded by the Foundation of Research, Science and Technology CO5XO207. The manuscript has benefited greatly from thorough reviews by Jeremy Richards, Stuart Simmons, and Jeff Mauk, and scientific and editorial comments by Larry Meinert.

Appendix I

Sample no.	Site	Rock description	NZMG East	NZMG North	RL (m)	Azimuth true N	Dip	EOH (m)
Bore hole samples								
SC1 3.07	Sams Creek, Main Zone	Quartz vein in granite	8973	1575	562.00	121	−45.0	84.10
SC1 3.07	Sams Creek, Main Zone	Quartz vein in granite	8973	1575	562.00	121	−45.0	84.10
SC4 221.3	Sams Creek, Main Zone	Arsenopyrite-pyrite veinlets in silicified microgranite	9030	1616	556.60	66	−45.0	19.50
SC4 228.25	Sams Creek, Main Zone	Contact metapelite/ carbonate-chlorite altered lamprophyre	9030	1616	556.60	66	−45.0	19.50
SC15 18.1	Sams Creek, Main Zone	Quartz vein in granite	8986	1593	461.42	331	−45.0	27.40
SC15 21.7	Sams Creek, Main Zone	Quartz vein in granite	8986	1593	461.42	331	−45.0	27.40
SC16 123.25	Sams Creek, Main Zone	Sulphide vein in granite	9008	1614	245.44	331	−55.0	213.75
SC16 4.65	Sams Creek, Main Zone	Sulphide vein in granite	9012	1614	245.44	331	−55.0	213.75
SC16 9.9	Sams Creek, Main Zone	Quartz-sulfide veins in silicified microgranite	9012	1614	245.44	331	−55.0	213.75
SC16A 15.0	Sams Creek, Main Zone	Sulphide vein in granite	9012	1614	245.44	311	−45.0	32.90
SC16A 20.9	Sams Creek, Main Zone	Sulphide vein in granite	9012	1614	245.44	311	−45.0	32.90
SC16A 26.18	Sams Creek, Main Zone	Sulphide vein in granite	9012	1614	245.44	311	−45.0	32.90
SC17A 10.2	Sams Creek, Main Zone	Sulphide vein in granite	9012	1614	245.44	331	−70.0	28.90
SC18 13.55	Sams Creek, Main Zone	Quartz-sulfide veins in silicified microgranite	9004	1605	315.00	321	−60.0	62.40
SC19 226.8	Sams Creek, Main Zone	Carbonate-quartz vein in granite	9009	1607	288.87	331	−45.0	230.00
SC25 137.75	Sams Creek, Main Zone	Porphyry granite	8992	1598	398.00	331	−47.5	250.00
SC25 138.0	Sams Creek, Main Zone	Carbonate-quartz vein in granite	8992	1598	398.00	331	−47.5	250.00
SC25 144.2	Sams Creek, Main Zone	Carbonate-quartz vein in granite	8992	1598	398.00	331	−47.5	250.00
SC25 147.0	Sams Creek, Main Zone	Quartz vein in granite	8992	1598	398.00	331	−47.5	250.00
SC25 151.7	Sams Creek, Main Zone	Carbonate-quartz vein in granite	8992	1598	398.00	331	−47.5	250.00
SC25 159.1	Sams Creek, Main Zone	Carbonate-sulphide vein in granite	8992	1598	398.00	331	−47.5	250.00
SC25 171.0	Sams Creek, Main Zone	Carbonate vein in granite	8992	1598	398.00	331	−47.5	250.00
SC25 171.1	Sams Creek, Main Zone	Quartz vein in granite	8992	1598	398.00	331	−47.5	250.00
SC25 174.8	Sams Creek, Main Zone	Sulphide vein in granite	8992	1598	398.00	331	−47.5	250.00
SC25 176.0	Sams Creek, Main Zone	Carbonate vein in granite	8992	1598	398.00	331	−47.5	250.00
SC25 176.4	Sams Creek, Main Zone	Carbonate vein in granite	8992	1598	398.00	331	−47.5	250.00
SC25 177.65	Sams Creek, Main Zone	Sulphide vein in granite	8992	1598	398.00	331	−47.5	250.00
SC25 203.1	Sams Creek, Main Zone	Quartz-sulfide veins in silicified microgranite	8992	1598	398.00	331	−47.5	250.00
SC25 203.5	Sams Creek, Main Zone	Quartz-sulfide veins in silicified microgranite	8992	1598	398.00	331	−47.5	250.00
SC25 218.5	Sams Creek, Main Zone	Phyllite	8992	1598	398.00	331	−47.5	250.00
SC26 101.1	Sams Creek, Main Zone	Sulphide vein in granite	9008	1598	231.53	-	−90.0	200.20
SC26 121.8	Sams Creek, Main Zone	Sulphide vein in granite	9008	1614	232.53	-	−90.0	200.20
SC29 29.8	Sams Creek, Main Zone	Quartz-sulfide veins in silicified microgranite	8788	1677	811.00	241	−45.0	121.10
SC29 30.7	Sams Creek, Riordans	Porphyry granite	8788	1677	811.00	241	−45.0	121.10
SC29 41.3	Sams Creek, Riordans	Quartz-sulfide veins in microgranite	8788	1677	811.00	241	−45.0	121.10
SC29 45.8	Sams Creek, Riordans	Quartz-sulfide veins in microgranite	8788	1677	811.00	241	−45.0	121.10
SC29 46.1	Sams Creek, Riordans	Quartz-sulfide veins in microgranite	8788	1677	811.00	241	−45.0	121.10
SC29 56.5	Sams Creek, Riordans	Quartz-sulfide veins in microgranite	8788	1677	811.00	241	−45.0	121.10

Sample no.	Site	Rock description	NZMG East	NZMG North	RL (m)	Azimuth true N	Dip	EOH (m)
SC29 61.8	Sams Creek, Riordans	Cataclasite at metasediment/ microgranite contact	8788	1677	811.00	241	−45.0	121.10
SC29 118.3	Sams Creek, Riordans	Quartz vein in metapelite	8788	1677	811.00	241	−45.0	121.10
SC29 120.5	Sams Creek, Riordans	Quartz-carbonate vein in metapelite	8788	1677	811.00	241	−45.0	121.10
SC29 120.9	Sams Creek, Riordans	Metapelite	8788	1677	811.00	241	−45.0	121.10
SC32 16.8	Sams Creek, SE Traverse	Quartz-sulfide veins in microgranite	8947	1529	505.00	151	−45.0	91.20
SC36 10.7	Sams Creek, Main Zone	Sulphide vein in granite	9012	1614	245.44	151	−45.0	203.00
SC36 26.2	Sams Creek, Main Zone	Porphyry granite	9012	1614	245.44	151	−45.0	203.00
SC37 94.3	Sams Creek, Doyles	Quartz-sulfide veins in sericite-altered microgranite	8893	1564	740.00	151	−65.0	142.80
SC37 94.4	Sams Creek, Doyles	Quartz-sulfide veins in sericite-altered microgranite	8893	1564	740.00	151	−65.0	142.80
SC37 95.5	Sams Creek, Doyles	Quartz-sulfide veins in sericite-altered microgranite	8893	1564	740.00	151	−65.0	142.80
SC37 88.5	Sams Creek, Doyles	Microgranite, sericite altered	8893	1564	740.00	151	−65.0	142.80
SC37 102.6	Sams Creek, Doyles	Porphyry granite	8893	1564	740.00	151	−65.0	142.80
SC37 104.0	Sams Creek, Doyles	Quartz-sulfide veins in sericite-altered microgranite	8893	1564	740.00	151	−65.0	142.80
SC37 108.6	Sams Creek, Doyles	Silicified microgranite	8893	1564	740.00	151	−65.0	142.80
SC38 7.3	Sams Creek, Doyles	Quartz-carbonate-sulfide veins in sericite-altered microgranite	8880	1562	735.00	201	−65.0	115.20
SC38 7.6	Sams Creek, Doyles	Quartz-sulfide veins in sericite-altered microgranite	8880	1562	735.00	201	−65.0	115.20
SC38 4.6	Sams Creek, Doyles	Microgranite, sericite altered	8880	1562	735.00	201	−65.0	115.20
SC38 17.5	Sams Creek, Doyles	Microgranite with disseminated carbonate	8880	1562	735.00	201	−65.0	115.20
SC39 29.6	Sams Creek, Main Zone	Quartz-sulfide veins in altered microgranite	8841	1608	787.00	241	−65.0	219.00
SC39 31.1	Sams Creek, Main Zone	Quartz-sulfide veins in altered microgranite	8841	1608	787.00	241	−65.0	219.00
SC39 39.2	Sams Creek, Western Outcrops	Porphyry granite	8841	1608	787.00	241	−65.0	219.00
SC39 47.0	Sams Creek, Main Zone	Quartz-sulfide veins in sericite-altered microgranite	8841	1608	787.00	241	−65.0	219.00
SC39 50.3	Sams Creek, Main Zone	Porphyry granite	8841	1608	787.00	241	−65.0	219.00
SC39 52.5	Sams Creek, Main Zone	Quartz-sulfide veins in silicified microgranite	8841	1608	787.00	241	−65.0	219.00
SC39 54.7	Sams Creek, Main Zone	Quartz-carbonate veins in silicified microgranite	8841	1608	787.00	241	−65.0	219.00
SC40 95.9	Sams Creek, Main Zone	Quartz-chlorite-carbonate vein in metasandstone	9030	1616	327.00	241	−65.0	195.80
SC40 104.0	Sams Creek, Main Zone	Quartz-carbonate vein in metasandstone	9030	1616	327.00	241	−65.0	195.80
SC40 105.5	Sams Creek, Main Zone	Quartz vein in metasandstone	9030	1616	327.00	241	−65.0	195.80
SC40 108.9	Sams Creek, Main Zone	Metasandstone with metapelite beds	9030	1616	327.00	241	−65.0	195.80
SC40 109.3	Sams Creek, Main Zone	Carbonate-chlorite altered lamprophyre	9030	1616	327.00	241	−65.0	195.80
SC40 109.6	Sams Creek, Main Zone	Carbonate-chlorite altered lamprophyre	9030	1616	327.00	241	−65.0	195.80
SC40 109.8	Sams Creek, Main Zone	Carbonate-chlorite altered lamprophyre	9030	1616	327.00	241	−65.0	195.80
SC40 111.2	Sams Creek, Main Zone	Hornfels/microgranite contact	9030	1616	327.00	241	−65.0	195.80
SC40 113.55	Sams Creek, Main Zone	Magnetite altered microgranite	9030	1616	327.00	241	−65.0	195.80
SC40 115.45	Sams Creek, Main Zone	Porphyry granite	9030	1616	327.00	241	−65.0	195.80
SC40 117.0	Sams Creek, Main Zone	Sulfide veins in silicified microgranite	9030	1616	327.00	241	−65.0	195.80
SC40 121.6	Sams Creek, Main Zone	Carbonate-quartz vein in granite	9030	1616	327.00	241	−65.0	195.80
SC40 121.7	Sams Creek, Main Zone	Quartz vein in granite	9030	1616	327.00	241	−65.0	195.80
SC40 122.3	Sams Creek, Main Zone	Metapelite contact with carbonate altered lamprophyre	9030	1616	327.00	241	−65.0	195.80
SC40 138.2	Sams Creek, Main Zone	Quartz vein in granite	9030	1616	327.00	241	−65.0	195.80
SC40 139.0	Sams Creek, Main Zone	Sulfide veins in silicified microgranite	9030	1616	327.00	241	−65.0	195.80
SC40 142.9	Sams Creek, Main Zone	Porphyry granite	9030	1616	327.00	241	−65.0	195.80
SC40 151.6	Sams Creek, Main Zone	Porphyry granite	9030	1616	327.00	241	−65.0	195.80
SC40 154.5	Sams Creek, Main Zone	Carbonate-altered granite	9030	1616	327.00	241	−65.0	195.80
SC40 155.0	Sams Creek, Main Zone	Carbonate-chlorite altered lamprophyre	9030	1616	327.00	241	−65.0	195.80
SC42 195.5	Sams Creek, Anvil	Silicified microgranite with sulfide and carbonate blebs	9051	1611	220.00	310	−50.0	288.00
SC42 186.4	Sams Creek, Anvil	Sulfide veins in silicified microgranite	9051	1611	220.00	310	−50.0	288.00
SC42 199.5	Sams Creek, Anvil	Quartz veins in magnetite-altered microgranite	9051	1611	220.00	310	−50.0	288.00
SC42 209.9	Sams Creek, Anvil	Sulfide veins in silicified microgranite	9051	1611	220.00	310	−50.0	288.00
SC42 210.3	Sams Creek, Anvil	Sulfide veins in silicified microgranite	9051	1611	220.00	310	−50.0	288.00
SC42 216.7	Sams Creek, Anvil	Quartz veins in magnetite-altered microgranite	9051	1611	220.00	310	−50.0	288.00
SC42 222.6	Sams Creek, Anvil	Silicified microgranite with sulfide and carbonate blebs	9051	1611	220.00	310	−50.0	288.00

Sample no.	Site	Rock description	NZMG East	NZMG North	RL (m)	Azimuth true N	Dip	EOH (m)
SC42 223.1	Sams Creek, Anvil	Silicified microgranite with sulfide and carbonate blebs	9051	1611	220.00	310	−50.0	288.00
SC42 229.2	Sams Creek, Anvil	Silicified microgranite with sulfide and carbonate blebs	9051	1611	220.00	310	−50.0	288.00
SC42 237.7	Sams Creek, Anvil	Silicified microgranite with sulfide and carbonate blebs	9051	1611	220.00	310	−50.0	288.00
SC42 246.8	Sams Creek, Anvil	Silicified microgranite with sulfide and carbonate blebs	9051	1611	220.00	310	−50.0	288.00
SC42 251.1	Sams Creek, Anvil	Silicified microgranite with sulfide and carbonate blebs	9051	1611	220.00	310	−50.0	288.00
SC42 256.4	Sams Creek, Anvil	Sulfide veins in silicified microgranite	9051	1611	220.00	310	−50.0	288.00
SC42 258.4	Sams Creek, Anvil	Silicified microgranite with sulfide and carbonate blebs	9051	1611	220.00	310	−50.0	288.00
SC42 285.7	Sams Creek, Anvil	Carbonate-chlorite-sericite altered lamprophyre	9051	1611	220.00	310	−50.0	288.00
SC43 12.0	Sams Creek, Main Zone	Pyritic metapelite	8982	1590	461.00	344	−57.0	129.40
SC43 61.5	Sams Creek, Main Zone	Carbonate veins in silicified microgranite	8982	1590	461.00	344	−57.0	129.40
SC43 46.0	Sams Creek, Main Zone	Silicified microgranite	8982	1590	461.00	344	−57.0	129.40
SC43 62.1	Sams Creek, Main Zone	Magnetite altered microgranite	8982	1590	461.00	344	−57.0	129.40
SC43 73.8	Sams Creek, Main Zone	Quartz-carbonate vein in silicified microgranite	8982	1590	461.00	344	−57.0	129.40
SC43 96.0	Sams Creek, Main Zone	Carbonate veins in silicified microgranite	8982	1590	461.00	344	−57.0	129.40
SC43 98.6	Sams Creek, Main Zone	Carbonate-chlorite altered lamprophyre	8982	1590	461.00	344	−57.0	129.40
SC43 113.3	Sams Creek, Main Zone	Pyritic metapelite	8982	1590	461.00	344	−57.0	129.40
SC43 114.0	Sams Creek, Main Zone	Pyritic metapelite	8982	1590	461.00	344	−57.0	129.40
SC43 115.9	Sams Creek, Main Zone	Quartz vein in metapelite	8982	1590	461.00	344	−57.0	129.40
SC43 121.0	Sams Creek, Main Zone	Pyritic metapelite	8982	1590	461.00	344	−57.0	129.40
SC44 136.5	Sams Creek, Main Zone	Metapelite with bedded pyrite	9008	1622	230.00	331	−73.0	329.30
SC44 173.3	Sams Creek, Main Zone	Carbonate-chlorite altered lamprophyre with carbonate veinlets	9008	1622	230.00	331	−73.0	329.30
SC44 174.2	Sams Creek, Main Zone	Silicified microgranite with sulphide and carbonate veinlets	9008	1622	230.00	331	−73.0	329.30
SC44 179.3	Sams Creek, Main Zone	Carbonate-chlorite altered lamprophyre	9008	1622	230.00	331	−73.0	329.30
SC44 184.6	Sams Creek, Main Zone	Silicified microgranite with sulphide and carbonate veinlets	9008	1622	230.00	331	−73.0	329.30
SC44 186.9	Sams Creek, Main Zone	Silicified microgranite with sulphide and carbonate veinlets	9008	1622	230.00	331	−73.0	329.30
SC44 195.7	Sams Creek, Main Zone	Silicified microgranite with sulphide and carbonate veinlets	9008	1622	230.00	331	−73.0	329.30
SC44 197.7	Sams Creek, Main Zone	Sericite-carbonate altered microgranite with quartz and sulphide veinlets	9008	1622	230.00	331	−73.0	329.30
SC44 226.3	Sams Creek, Main Zone	Arsenopyrite vein in silicified microgranite	9008	1622	230.00	331	−73.0	329.30
SC44 234.0	Sams Creek, Main Zone	Arsenopyrite-pyrite veinlets in silicified microgranite	9008	1622	230.00	331	−73.0	329.30
SC44 246.8	Sams Creek, Main Zone	Arsenopyrite vein with fringe of black ?sulphide in silicified microgranite	9008	1622	230.00	331	−73.0	329.30
SC44 251.6	Sams Creek, Main Zone	Arsenopyrite-pyrite veinlets in silicified microgranite	9008	1622	230.00	331	−73.0	329.30
SC44 276.0	Sams Creek, Main Zone	Arsenopyrite-pyrite veinlets in silicified microgranite	9008	1622	230.00	331	−73.0	329.30
SC44 276.2	Sams Creek, Main Zone	carbonate + feldspar vein in silicfied microgranite	9008	1622	230.00	331	−73.0	329.30
SC44 318.2	Sams Creek, Main Zone	Cemented fault breccia with clasts of lamprophyre and metapelite	9008	1622	230.00	331	−73.0	329.30
SC44 327.0	Sams Creek, Main Zone	Metapelite with disseminated pyrite	9008	1622	230.00	331	−73.0	329.30
SC45 54.2	Sams Creek, Main Zone	Metasandstone with carbonate alteration	9008	1622	231.00	91	−60.0	148.85
SC45 63.8	Sams Creek, Main Zone	Carbonate-chlorite-sericite altered lamprophyre	9008	1622	231.00	91	−60.0	148.85
SC45 65.2	Sams Creek, Main Zone	Carbonate-chlorite altered lamprophyre	9008	1622	231.00	91	−60.0	148.85
SC45 67.3	Sams Creek, Main Zone	Carbonate veinlets in silicified microgranite	9008	1622	231.00	91	−60.0	148.85
SC45 69.7	Sams Creek, Main Zone	Arsenopyrite vein cut by pyrite veinlets in silicified microgranite	9008	1622	231.00	91	−60.0	148.85
SC45 72.6	Sams Creek, Main Zone	Sericite-quartz alteration replacing magnetite alteration	9008	1622	231.00	91	−60.0	148.85

Sample no.	Site	Rock description	NZMG East	NZMG North	RL (m)	Azimuth true N	Dip	EOH (m)
SC45 92.0	Sams Creek, Main Zone	Arsenopyrite-pyrite veinlets in silicified microgranite	9008	1622	231.00	91	−60.0	148.85
SC45 93.6	Sams Creek, Main Zone	Arsenopyrite-pyrite veinlets in silicified microgranite	9008	1622	231.00	91	−60.0	148.85
SC45 112.1	Sams Creek, Main Zone	Contact carbonate-rich lamprophyre/silicfied granite with pyrite veinlets	9008	1622	231.00	91	−60.0	148.85
SC45 112.2	Sams Creek, Main Zone	Carbonate-chlorite altered lamprophyre	9008	1622	231.00	91	−60.0	148.85
SC45 112.8	Sams Creek, Main Zone	Carbonate-chlorite-sericite altered lamprophyre	9008	1622	231.00	91	−60.0	148.85
SC45 115.6	Sams Creek, Main Zone	Carbonate-rich lamprophyre cutting metapelite	9008	1622	231.00	91	−60.0	148.85
SC45 118.1	Sams Creek, Main Zone	Breccia with clasts of metapelite, vein quartz and pyrite	9008	1622	231.00	91	−60.0	148.85
SC45 119.0	Sams Creek, Main Zone	Quartz vein in metapelite	9008	1622	231.00	91	−60.0	148.85
SC48 187.15	Sams Creek, Main Zone	Quartz vein	9030	1616	329.80	312	−75.0	248.70
SC48 187.2	Sams Creek, Main Zone	Contact carbonate-rich lamprophyre/silicfied microgranite	9030	1616	329.80	312	−75.0	248.70
SC48 190.2	Sams Creek, Main Zone	Carbonate vein in silicified microgranite	9030	1616	329.80	312	−75.0	248.70
SC48 190.4	Sams Creek, Main Zone	Sphalerite in sulphide vein in silicified microgranite	9030	1616	329.80	312	−75.0	248.70
SC48 198.4	Sams Creek, Main Zone	Arsenopyrite-pyrite veinlets in silicified microgranite	9030	1616	329.80	312	−75.0	248.70
SC48 201.4	Sams Creek, Main Zone	Silicified microgranite veined with quartz, sulphide and carbonate	9030	1616	329.80	312	−75.0	248.70
SC48 203.4	Sams Creek, Main Zone	Sericite-rich microgranite veined with quartz, sulphide and carbonate	9030	1616	329.80	312	−75.0	248.70
SC48 206.8	Sams Creek, Main Zone	Arsenopyrite-pyrite veinlets in silicified microgranite	9030	1616	329.80	312	−75.0	248.70
SC48 207.7	Sams Creek, Main Zone	Magnetite altered microgranite with quartz veinlets	9030	1616	329.80	312	−75.0	248.70
SC48 221.3	Sams Creek, Main Zone	Arsenopyrite-pyrite veinlets in silicified microgranite	9030	1616	329.80	312	−75.0	248.70
SC48 222.0	Sams Creek, Main Zone	Carbonate veinlets in silicified microgranite	9030	1616	329.80	312	−75.0	248.70
SC48 228.3	Sams Creek, Main Zone	Carbonate-chlorite altered lamprophyre with quartz-carbonate-sulphide veinlets	9030	1616	329.80	312	−75.0	248.70
SC48 228.3	Sams Creek, Main Zone	Carbonate-chlorite altered lamprophyre with quartz-carbonate-sulphide veinlets	9030	1616	329.80	312	−75.0	248.70
SC48 240.2	Sams Creek, Main Zone	Metapelite with quartz-pyrite veinlets	9030	1616	329.80	312	−75.0	248.70
Outcop Samples								
P68911	Sams Creek, Main Zone	Silicified microgranite	8980	1580				
P68912	Sams Creek, Anvil	Porphyry granite	9120	1620				
P68913	Sams Creek, Barrons Flat	Porphyry granite	9260	1660				
P68914	Sams Creek, Barrons Flat	Porphyry granite	9210	1610				
P68915	Cobb Dam Road	Devil River Group; greenschist, sulfide-rich	8770	1350				
CN 1078	Arthur Marble	Metamorphosed marine carbonate with trace pyrite	Locality indicated on Fig. 1					
CN 1079	Arthur Marble	Metamorphosed marine carbonate with trace pyrite	Locality indicated on Fig. 1					
CN 632	Arthur Marble	Metamorphosed marine carbonate with trace pyrite	Locality indicated on Fig. 1					
CN 652	Arthur Marble	Metamorphosed marine carbonate with trace pyrite	Locality indicated on Figure 1					

References

Bottinga Y (1969) Calculated fractionation factors for carbon and hydrogen isotope exchange in the system calcite-carbon dioxide-graphite-methane-hydrogen-water vapor. Geochimica et Cosmochimica Acta 33:49–64

Boutton TW (1991) Stable carbon isotope ratios of natural materials: I. Sample preparation and mass spectrometric analysis In: Coleman DC, Fry B (eds) Carbon Isotope Techniques. Academic Press, pp 155–171

Bradshaw MA (2000) Base of the Devonian Baton Formation and the question of a pre-Baton tectonic event in the Takaka Terrane, NZ J Geol Geophys 43:601–610

Brathwaite RL, Faure K (2004) The Sams Creek peralkaline granite hosted gold deposit, Northwest Nelson, New Zealand: a new variant on alkaline intrusion-related gold deposits, Proc PACRIM Cong, pp 273–274

Brathwaite RL, Kamo S, Faure K (2004) U-Pb geochronology and geochemistry of molybdenum-bearing granodiorite porphyry at Copperstain Creek, west Nelson, New Zealand. NZ J Geol Geophys 47:219–225

Brathwaite RL, Pirajno F (1993) Metallogenic map of New Zealand: Monograph 3. Institute of Geological & Nuclear Sciences, Lower Hutt, p 215

Carothers WW, Adami LH, Rosenbauer RJ (1988) Experimental oxygen isotope fractionation between siderite-water and phosphoric acid liberated CO_2 -siderite. Geochimica et Cosmochimica Acta 52:2445–2450

Chacko T, Cole DR, Horita J (2001) Equilibrium oxygen, hydrogen and carbon isotope fractionation factors applicable to geologic systems. Stable isotope geochemistry In: Valley JW, Cole DR (eds) Rev Mineral Geochem 43:1–81

Challis GA, Grapes R, Palmer K (1995) Chromium muscovite, uvarovite, and zincian chromite: products of regional metasomatism in northwest Nelson, New Zealand. Canad Mineral 33:1263–1284

Chaussidon M, Albarede F, Sheppard SMF (1987) Sulfur isotope heterogeneity in the mantle from ion microprobe measurements of sulphide inclusions in diamonds. Nature 330:242–244

Clayton RN, Kieffer SW (1991) Oxygen isotopic thermometer calibrations In: Taylor HP Jr, O'Neil JR, Kaplan IR (eds) Stable isotope geochemistry; a tribute to Samuel Epstein, pp 3–10

Clayton RN, O'Neil JR, Mayeda TK (1972) Oxygen isotope exchange between quartz and water. J Geophys Res 77:3057–3067

Clementson IM (1987) Takaka River PL 31–1195 and Cobb River PL 31–1196, Sams Creek project, report on exploration March 1985 to May 1987. CRA Exploration Pty Ltd, Ministry of Economic Development, Wellington, unpublished open file mineral report MR1014

Collins PLF (1979) Gas hydrates in CO_2-bearing fluid inclusions and the use of freezing data for estimation of salinity. Econ Geol 74:1435–1444

Collins WJ, Beams SD, White AJR, Chappell BW (1982) Nature and origin of A-type granites with particular reference to southeastern Australia. Contrib Mineral Petrol 80:189–200

Cooper RA (1989) Early Paleozoic terranes of New Zealand. J Roy Soc NZ 19:73–112

Cooper RA, Tulloch AJ (1992) Early Palaeozoic terranes in New Zealand and their relationship to the Lachlan Fold Belt. Tectonophysics 214:129–144

Craw D, Hall AJ, Fallick AE, Boyce AJ (1995) Sulphur isotopes in a metamorphogenic gold deposit, Macraes Mine, Otago Schist, New Zealand. NZ J Geol Geophys 38:131–136

Criss RE, Ekren EB, Hardyman RF (1984) Casto ring zone; a 4,500-km^2 fossil hydrothermal system in the Challis volcanic field, central Idaho. Geology 12:331–334

Deines P (2002) The carbon isotope geochemistry of mantle xenoliths. Earth-Sci Rev 58:247–278

de Ronde CEJ, Sibson RH, Bray CJ, Faure K (2001) Fluid chemistry of veining associated with an ancient microearthquake swarm, Benmore Dam, New Zealand. Geol Soc Am Bull 113:1010–1024

Diamond LW (2003) Introduction to gas-bearing aqueous fluid inclusions In: Sanson I, Anderson A, Marshall D (eds) Fluid inclusions: analysis and interpretation. Mineral Assoc Can Short Course Ser 32:101–158

Eldridge CS, Compston W, Williams IS, Harris JW, Bristow JW (1991) Isotope evidence for the involvement of recycled sediments in diamond formation. Nature 353:649–653

Faure K, Brathwaite RL, de Ronde CEJ (2003) Gold mineralisation in the polymetallic Sams Creek peralkaline microgranite, South Island, New Zealand. Proc Geofluids IV, J Geochem Exp 78–79:613–616

Giles AD, Marshall B (1994) Fluid inclusion studies on a multiply deformed, metamorphosed volcanic-associated massive sulfide deposit, Joma Mine, Norway. Econ Geol 89:803–819

Giletti BJ (1986) Diffusion effects on oxygen isotope temperatures of slowly cooled igneous and metamorphic rocks. Earth Planet Sci Lett 77:218–228

Golyshev SI, Padalko NL, Pechenkin SA (1981) Fractionation of stable isotope oxygen and carbon in carbonate systems. Geochem Int 18:85–99

Gregory RT, Criss RE, Taylor HP Jr (1989) Oxygen isotope exchange kinetics of mineral pairs in closed and open systems; applications to problems of hydrothermal alteration of igneous rocks and Precambrian iron formations. Chem Geol 75:1–42

Grindley GW (1978) Late Precambrian-Devonian startigraphy and Tuhua Orogeny In: Suggate RP, Stevens GR, Te Punga MT (eds) Geology of New Zealand. Dept of Scientific and Industrial Research, Wellington, 80–90 and 124–132

Grindley GW (1980) Sheet S13–Cobb. Geological map of New Zealand, Dept of Scientific and Industrial Research, Wellington, 46p

Harmon RS, Hoefs J (1986) S-isotope relationships in late Cenozoic destructive plate margin and continental intraplate volcanic rocks. Terra Cognita 6:182

Harmon RS, Hoefs J, Wedepohl KH (1987) Stable isotope (O, H, S) relationships in Tertiary basalts and their mantle xenoliths from the northern Hessian Depression, W.-Germany. Contrib Mineral Petrol 95:350–369

Harris C (1995) Oxygen isotope geochemistry of the Mesozoic anorogenic complexes of Damaraland, Northwest Namibia; evidence for crustal contamination and its effect on silica saturation. Contrib Mineral Petrol 122:308–321

Harris C, Faure K, Diamond RE, Scheepers R (1997) Oxygen and hydrogen isotope geochemistry of S- and I-type granitoids: the Cape Granite suite, South Africa. Chem Geol 143:96–114

Hickey KA (1986) Geology of Paleozoic and Tertiary rocks between Upper Takaka and the Waingaro River, north-west Nelson. Unpublished MSc Thesis, University of Auckland, Auckland

Hogan JP, Gilbert MC (1995) The A-type Mount Scott Granite sheet: The importance of crustal magma traps. J Geophys Res, Planets 100, No. B8: 15779–15792

Ionov DA, Hoefs J, Wedepohl KH, Wiechert U (1992) Content and isotopic composition of sulphur in ultramafic xenoliths from Central Asia. Earth Planet Sci Lett 111:269–286

Ishihara S (1981) The granitoid series and mineralization. Econ Geol, Seventy-fifth anniversary volume: 458–484

Ishihara S, Jin M-S, Sasaki A (2000) Source diversity of ore sulfur from Mesozoic-Cenozoic mineral deposits in the Korean Peninsula region. Res Geol 50:203–212

Ishihara S, Sasaki A (2002) Paired sulfur isotopic belts: Late Cretaceous-Paleogene ore deposits of Southwest Japan. Bull Geol Sur Jpn 53:461–477

Ishihara S, Murakami H (2004) Granitoid types related to Cretaceous plutonic Au-quartz vein and Cu-Fe skarn deposits, Kitakami mountains, Japan. Res Geol 54:281–298

Javoy M, Weis D (1987) Oxygen isotopic composition of alkaline anorogenic granites as a clue to their origin; the problem of crustal oxygen. Earth Planet Sci Lett 84:415–422

Jensen EP, Barton MD (2000) Gold deposits related to alkaline magmatism. In: Hagemann SG, Brown PE (eds) Gold in 2000. Rev in Econ Geol 13:279–314

Jongens R (1997) The Anatoki Fault and the structure of the adjacent Buller and Takaka Terrane rocks, Northwest Nelson, New Zealand. Unpublished PhD thesis, University of Canterbury, Christchurch. 383p

Jongens R (2004) East-directed thrusting across the Buller and Takaka terranes, Northwest Nelson. Geol Soc NZ Miscell Pub 117A:51–52

Kerrich R, Beckinsale RD, Durham JJ (1977) The transition between deformation regimes dominated by intercrystalline diffusion and intracrystalline creep evaluated by oxygen isotope geothermometry. Tectonophysics 38:241–258

Kyser TK (1986) Stable isotope variations in the mantle In: Valley JW, Taylor HP Jr, O'Neil JR (eds) Stable isotopes in high temperature geological processes, Rev Mineral v. 16, Mineralogical Society of America, pp 141–164

Lang JR, Baker T (2001) Intrusion-related gold systems: the present level of understanding. Mineralium Deposita 36:477–489

McCrea JM (1950) On the isotopic chemistry of carbonates and palaeo-temperature scale. J Chem Phys 18:849–857

Marsh EE, Goldfarb RJ, Hart CRJ, Johnson CA (2003) Geology and geochemistry of the Clear Creek intrusion-related gold occurrences, Tintina Gold Province, Yukon, Canada. Canad J Earth Sci 40:681–699

Marshall B, Giles AD, Hagemann SG (2000) Fluid inclusions in metamorphosed and synmetamorphic (including metamorphogenic) base and precious metal deposits: indicators of ore-forming conditions and/or ore-modifying histories? In: Spry PG, Marshall B, Vokes FM (eds) Metamorphosed and metamorphogenic ore deposits. Rev Econom Geol 11:119–148

Muir RJ, Weaver SD, Bradshaw JD, Eby GN, Evans JA (1995) The Cretaceous Separation Point Batholith, New Zealand; granitoid magmas formed by melting of mafic lithosphere. J Geol Soc Lond 152:689–701

Muir RJ, Ireland TR, Weaver SD, Bradshaw JD (1996) Ion microprobe dating of Paleozoic granitoids: Devonian magmatism in New Zealand and correlations with Australia and Antarctica. Chem Geol 127:191–210

Müller D, Groves DI (1993) Direct and indirect associations between potassic igneous rocks, shoshonites and gold-copper deposits. Ore Geol Rev 8:383–406

Münker C, Cooper R (1999) The Cambrian arc complex of the Takaka Terrane, New Zealand: an integrated stratigraphical, paleontological and geochemical approach. NZ J Geol Geophys 42:415–445

Oceana Gold Limited (2004) Prospectus. 174p

O'Hara KD, Sharp ZD, Moecher DP, Jenkin GRT (1997) The effect of deformation on oxygen isotope exchange in quartz and feldspar and significance of isotopic temperatures in mylonites. J Geol 105:193–204

Ohmoto H (1972) Systematics of Sulfur and Carbon Isotopes in Hydrothermal Ore Deposits. Econ Geol 67:551–578

Ohmoto H, Goldhaber MB (1997) Sulfur and carbon isotopes In: Barnes HL (ed) Geochemistry of hydrothermal ore deposits, pp 517–612

O'Neil JR, Chappell BW (1977) Oxygen and hydrogen isotope relations in the Berridale Batholith. J Geol Soc Lond 133:559–571

Poulson SR, Kubilius WP, Ohmoto H (1991) Geochemical behavior of sulfur in granitoids during intrusion of the South Mountain Batholith, Nova Scotia, Canada. Geochimica et Cosmochimica Acta 55:3809–3830

Rattenbury MS, Cooper RA, Johnston MR (1998) Geology of the Nelson area: 1:250 000 geological map 9. Institute of Geological & Nuclear Sciences, Lower Hutt, 67p

Reynolds L (2004) Exploration at the Sams Creek project, northwest Nelson, New Zealand. Proceedings of the 37th Annual Conference of the New Zealand Branch of the Australasian Institute of Mining and Metallurgy:27–336

Richards JP (1995) Alkalic-type gold deposits: a review In: Thompson JHF (ed) Magmas, Fluids and Ore Deposits. Mineral. Assoc. Canada, Short Course Vol. 23, pp 267–400

Richet P, Bottinga Y, Javoy M (1977) A review of hydrogen, carbon, nitrogen, oxygen, sulphur, and chlorine stable isotope fractionation among gaseous molecules. Ann Rev Earth Planet Sci 5:65–110

Robinson W, Kusakabe M (1975) Quantitative preparation of sulfur dioxide, for $^{34}S/^{32}S$ analyses, from sulfides by combustion with cuprous oxide. Anal Chem 47:1179–1181

Roedder E (1984) Fluid inclusions. Mineral Soc Am Rev Mineral Vol. 12

Rosenbaum J, Sheppard SMF (1986) An isotopic study of siderites, dolomites and ankerites at high temperatures. Geochimica et Cosmochimica Acta 50:1147–1150

Rowins SM (2000) Reduced porphyry copper-gold deposits: a new variation on an old theme. Geology 28:491–494

Sasaki A, Arikawa Y, Folinsbee RE (1979) Kiba reagent method of sulfur extraction applied to isotopic work. Bull Geol Sur Jpn 30:1179–1181

Schneider A (1970) The sulfur isotope composition of basaltic rocks. Contrib Mineral Petrol 25:95–124

Sharp ZD (1990) Laser-based microanalytical method for the in situ determination of oxygen isotope ratios of silicates and oxides. Geochimica et Cosmochimica Acta 54:1353–1357

Shelley D (1984) Takaka River recumbent fold complex, Nelson, New Zealand. NZ J Geol Geophy 27:139–149

Shepherd TJ, Rankin AH, Alderton DHM (1985) A practical guide to fluid inclusion studies. Blackie and Son, Glasgow

Sheppard SMF (1986) Characterization and isotopic variations in natural waters In: Valley JW, Taylor HPJ, O'Neil JR (eds) Stable isotope in high temperature geological processes. Rev Mineral v. 16, Mineralogical Society of America, pp 165–183

Sillitoe RH (2000) Gold-rich porphyry deposits; descriptive and genetic models and their role in exploration and discovery In: Hagemann SG, Brown PE (eds) Gold in 2000. Rev Econ Geol 13:315–345

Taylor HPJ, Sheppard SMF (1986) Igneous rocks: I Processes of isotopic fractionation and isotope systematics. In: Valley JW, Taylor HPJ, O'Neil JR (eds) Stable isotope in high temperature geological processes. Brookcrafters Inc., Michigan, pp 227–271

Thiéry R, van den Kerkhof AM, Dubessy J (1994) VX properties of CH_4 -CO_2 and CO_2 -N_2 fluid inclusions; modelling for $T < 31°C$ and $P < 400$ bars. Eur J Mineral 6:753–771

Thompson JFH, Newberry RJ (2000) Gold deposits related to reduced granitic intrusions In: Hagemann SG, Brown PE (eds) Gold in 2000. Rev Econ Geol 13:377–400

Tulloch AJ (1983) Granitoid rocks of New Zealand; a brief review. In: Roddick JA (ed) Circum-Pacific Plutonic Terranes. Memoir–Geological Society of America 159:5–20

Tulloch AJ (1992) Petrology of the Sams Creek peralkaline granite dike, Takaka, New Zealand. NZ J Geol Geophys 35:193–200

Tulloch AJ, Dunlap WJ (submitted) A Carboniferous $^{40}Ar/^{39}Ar$ amphibole emplacement age for the Au-bearing Sams Creek alkali-feldspar granite dike, west Nelson, New Zealand. NZ J Geol Geophys

Tulloch AJ, Kimborough DL, Faure K, Allibone AH (2003) Paleozoic plutonism in the New Zealand sector of Gondwana In: Blevin P, Jones M, Chappell (eds) Magmas to mineralisation: the Ishihara symposium. Geoscience Australia, Macquarie University, pp 123–124

Tulloch AJ, Kimbrough DL (2003) Paired plutonic belts in convergent margins and the development of high Sr/Y magmatism: the Peninsular Ranges Batholith of California and the Median Batholith of New Zealand. Tectonic evolution of northwestern Mexico and southwestern USA. Geol Soc Am Spl Paper 374:275–295

Tulloch AJ, Rabone SDC (1993) Mo-bearing granodiorite porphyry plutons of the Early Cretaceous Separation Point Suite, west Nelson, New Zealand. NZ J Geol Geophys 36:401–408

Turner SP, Foden JD, Deblond A, Duchesne JC (1992) Derivation of some A-type magmas by fractionation of basaltic magma: an example from the Padhaway Ridge, South Australia. Lithos 28:23–55

Veizer J, Ala D, Azmy K, Bruckschen P, Buhl D, Bruhn F, Carden GAF, Diener A, Ebneth S, Godderis Y (1999) $^{87}Sr/^{86}Sr$, $\delta^{13}C$ and $\delta^{18}O$ evolution of Phanerozoic seawater. Chem Geol 161:59–88

Voll G (1976) Recrystallization of quartz, biotite and feldspars from Erstfeld to the Leventina Nappe, Swiss Alps, and its geological significance. Schweizerische mineralogische und petrographische Mitteilungen 56:641–647

Whalen JB, Currie KL, Chappell BW (1987) A-type granites: geochemical characteristics, discrimination and petrogenesis. Contrib Mineral Petrol 95:407–419

Windle SJ (1989) The nature and origin of gold mineralisation at Sams Creek, North-west Nelson. Unpublished MSc, Thesis, University of Otago, Dunedin

Windle SJ, Craw D (1991) Gold mineralisation in a syntectonic granite dike, Sams Creek, Northwest Nelson, New Zealand. NZ J Geol Geophys 34:429–440

Wyman D, Kerrich R (1988) Alkaline magmatism, major structures, and gold deposits: implications for greenstone belt gold metallogeny. Econ Geol 83:454–461

Wyman D, Kerrich R (1989) Archean shoshonitic lamprophyres associated with Superior province gold deposits: distribution, tectonic setting, noble metal abundances, and significance for gold mineralization Economic Geology, Monograph 6. pp 651–667

Zhang CL, Horita J, Cole DR, Zhou J, Lovley DR, Phelps TJ (2001) Temperature-dependent oxygen and carbon isotope fractionations of biogenic siderite. Geochimica et Cosmochimica Acta 65:2257–2271

Zheng Y-F (1993) Calculation of oxygen isotope fractionation in anhydrous silicate minerals. Geochimica et Cosmochimica Acta 57:1079–1091

Zheng Y-F (1999) Oxygen isotope fractionation in carbonate and sulfate minerals. Geochem J 33:109–126